Natural Resources for Human Health

visagaa publishing house

Original Research

View Article online

Check for updates

Received 25 November 2025
Revised 13 January 2026
Accepted 25 January 2026
Available Online 13 July 2026

Edited by Shafi Ullah Khan

KEYWORDS:
Antioxidant
Molecular docking
Mpro
Neuraminidase
PLpro
Respiratory viruses

https://doi.org/10.53365/nrfhh/217343
eISSN: 2583-1194

In vitro and in silico antiviral activity of GC–MS-identified metabolites from three South African medicinal plants against H1N1 and SARS-CoV-2

Lesiba Thabo Lekgoathi[1], Sechene Stanley Gololo[1], Thankhoe Abram Rants'o[2], Lefa Julius Lerotholi[3], Xavier Siwe-Noundou[4], Vuyisile Samuel Thibane[1]*

[1]Department of Biochemistry and Biotechnology, Sefako Makgatho Health Sciences University, Ga-Rankuwa, South Africa
[2]Department of Pharmacology and Toxicology, University of Utah, Salt Lake City, UT, United States
[3]Department of Pharmacy and Pharmacology, University of Witwatersrand, Johannesburg, South Africa
[4]Department of Pharmaceutical Sciences, Sefako Makgatho Health Sciences University, Ga-Rankuwa, South Africa

ABSTRACT: Influenza A virus subtype H1N1 (H1N1) and severe acute respiratory syndrome coronavirus 2 (SARS-CoV-2) can both infect the respiratory tract and cause symptoms such as fever, cough, and shortness of breath. Medicinal plants offer an alternative treatment strategy, as they can provide relief against these respiratory-related viruses. The present study aimed to evaluate the antiviral activity and molecular modelling of metabolites from *Eucalyptus globulus* Labill., *Schinus molle* L., and *Searsia lancea* (L.f) F.A.Barkley. The detection and identification of volatile phytoconstituents in the extracts were performed by GC-MS analysis. The samples were further assessed through the in vitro activity screening and followed by molecular modelling-mediated prediction of bioactive constituents. Volatile compounds were identified in hexane extracts, with hydrocarbons accounting for the highest peak percentage across all three plant samples. Hexane extracts from all three plants demonstrated inhibitory activity, varying in potency, with *E. globulus* and *S. molle* extracts being highly potent (IC_{50} values < 100 µg/mL) against PLpro from SARS-CoV-2. Accordingly, the in silico study identified geranylgeranyl acetate from *S. molle* and 1-tetracosanol from both *E. globulus* and *S. molle* as potential inhibitors of the SARS-CoV-2 protease (PDB: 7MB1). Molecular dynamics revealed that they formed stable complexes with the SARS-CoV-2 protease and interacted with key active-site amino acid residues, including the catalytic site residues His41 and Cys145. The results of this study highlight the need to assess the efficacy of geranylgeranyl acetate and 1-tetracosanol against the SARS-CoV-2 protease in pharmacological in vitro and in vivo studies.

* Corresponding author.
E-mail address: vuyisile.thibane@smu.ac.za (Vuyisile Samuel Thibane)

GRAPHICAL ABSTRACT

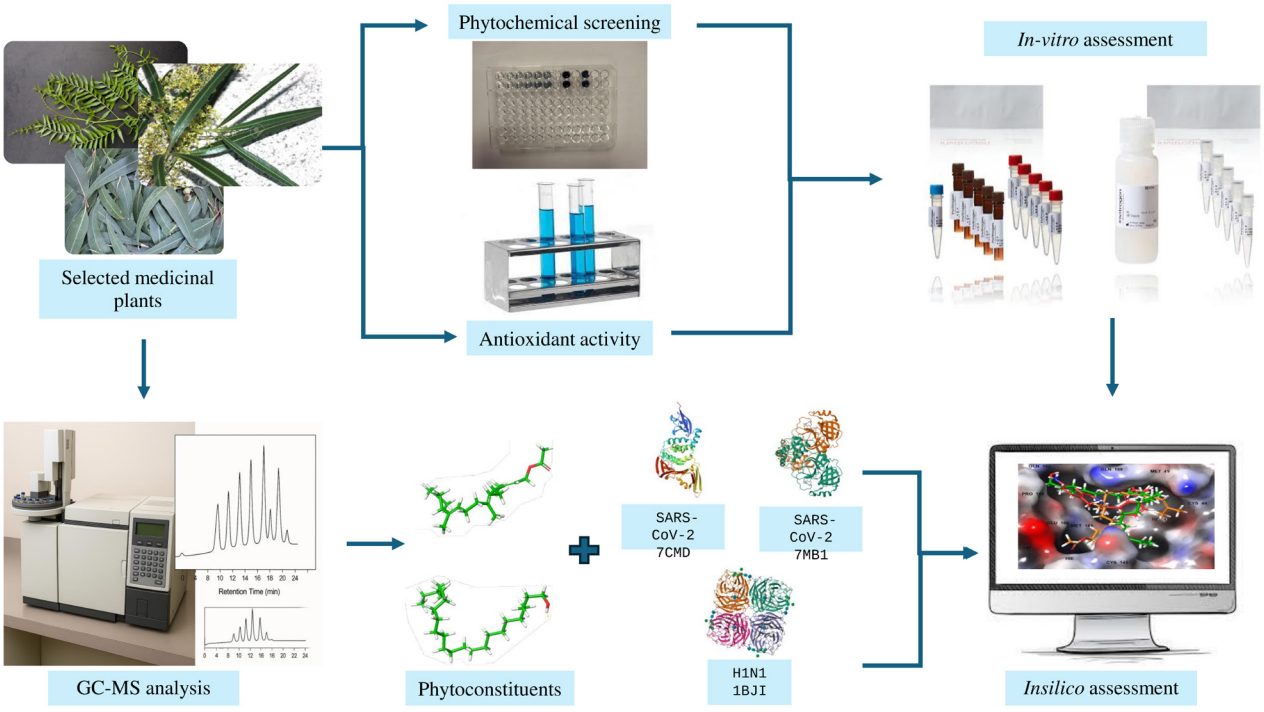

1. INTRODUCTION

Respiratory viruses are infectious agents that mainly affect the respiratory system, leading to a range of conditions from mild respiratory discomfort to severe respiratory illnesses (Weston and Frieman, 2018). Common symptoms include coughing, throat irritation, fever, nasal congestion, and, in severe instances, pneumonia and acute respiratory distress syndrome (ARDS) (Nelson et al., 2022). Notable viruses in this category include influenza viruses responsible for seasonal flu outbreaks and severe acute respiratory syndrome coronavirus 2 (SARS-CoV-2), which causes coronavirus disease (Jacek et al., 2021). Influenza viruses have in the past caused several pandemics, including the 2009 H1N1 pandemic (Girard et al., 2010). This was caused by the H1N1 strain of influenza A, which remains one of the predominant flu-season strains. There are multiple targets for combating influenza viruses, such as the H1N1 (Jhaveri, 2020). One of these targets includes neuraminidase, an important enzyme found on the surface of influenza viruses, including H1N1 (Minami et al., 2021). The primary function of this enzyme is to cleave sialic acid residues via a hydrolytic reaction that adds a water molecule, resulting in the separation of sialic acid from the host cell glycoprotein (Wallace et al., 2023). The SARS-CoV-2 virus, which previously led to the coronavirus disease 2019 (COVID-19) pandemic, has multiple targets for therapeutic intervention (McClain and Vabret, 2020). Two of these targets include the papain-like protease (PL^{pro}) and the main protease (Mpro) of SARS-CoV-2, which are essential enzymes involved in the replication and proliferation of the virus (Chia and Lim, 2023; Hu et al., 2022). It has a crucial function in the cleavage and development of viral polyproteins, formation of the replicase-transcriptase complex, and interference with host responses (Ghosh et al., 2023).

Current treatment regimens against influenza and SARS-CoV-2-related diseases face challenges such as the emergence of antiviral resistance, medication ineffectiveness, vaccine hesitancy and low uptake, potential side effects, and the continuous evolution of viral variants (Sanz-Leon et al., 2022). Aromatic medicinal plants contain essential oils that have been explored for their potential antiviral activity (Reichling, 2022). These plants are a rich source of secondary metabolites that exhibit antioxidant activity and thus enhance the plant's antiviral activity (Tsamo et al., 2021). Their antioxidant ability is due to the presence of at least one benzene ring in which a hydrogen atom is replaced by a hydroxyl group

(Shoker et al., 2023). Furthermore, the induction of antioxidant activity by phenolic compounds occurs through various mechanisms, such as free radical scavenging, metal chelation, promotion of antioxidant enzyme activity, and inhibition of pro-oxidant enzymes (Mathew et al., 2015). Some of these phenolic compounds have been reported to inactivate viruses by disrupting their lipid envelope (Oxford et al., 2005). Proliferation of respiratory viruses can disturb redox balance, ultimately leading to oxidative damage (Chen et al., 2020). This underscores the therapeutic potential of phenolic compounds in combating viral infections and disease. Therefore, the aim of this study was to evaluate selected plants commonly used for colds and influenza for their phytochemical content, antioxidant potential, and chemical composition, and to assess their antiviral properties against selected targets of H1N1 and SARS-CoV-2 viruses using in vitro and in silico analyses.

2. MATERIALS AND METHODS

2.1. Plant collection, extract preparation, and voucher specimen preparation

The plant materials were collected in Zebediela, Limpopo Province, South Africa with their coordinates represented in Table 1. The leaves of *Eucalyptus globulus* Labill. (*E. globulus*), *Schinus molle* L. (*S. molle*), and *Searsia lancea* (L.f) F.A.Barkley (*S. lancea*) were separated into batches and left to dry at room temperature . After drying, the samples were then ground into powder using a benchtop grinder and stored in brown bags/airtight containers until further use. The dried ground plant material was sequentially extracted with hexane, acetone, and 80% aqueous methanol (v/v) for 24 hours using an orbital shaker. All extracts were filtered through Whatman No. 1 filter paper, and the filtrates were concentrated using a rotary evaporator and left under vacuum with a steady flow of cool air until completely dry. Plant extracts were prepared in duplicates, and the experiment was repeated three times to ensure reproducibility of the results. Voucher specimens (Table 1) were prepared and kept at the departmental specimen collection depot held at Sefako Makgatho Health Sciences University (SMU).

Table 1
Coordinates of the collection sites for selected medicinal plants in Zebediela, Capricorn District Municipality, Limpopo Province, South Africa.

Name	Voucher specimen	Location
Eucalyptus globulus	ENLMP202401	24°26'52.1"S 29°19'55.5"E
Schinus molle	ENLMP202402	24°26'52.1"S 2919'55.5"E
Searsia lancea	ENLMP202403	24°27'19.9"S 2919'59.0"E

2.2. Phytochemical content analysis

2.2.1. Determination of the total phenolic content

The total phenolic content of the methanolic extracts was determined using the Folin–Ciocalteu (Folin-C) method as described by Tambe and Bhambar (2014). Briefly, extracts (50 µL; 1 mg/mL) were added to 950 µL of sterile distilled water in separate glass test tubes. Folin-Ciocalteu reagent solution (500 µL; 1N) and 2.5 mL of sodium carbonate (2%, w/v) were added to the reaction mixture, which was incubated at room temperature for 40 minutes. Gallic acid was used as a positive control, while a reaction mixture containing 80% aqueous methanol (v/v) was used as a negative control. The samples were then transferred to a 96-well plate, and the absorbance was read at 725nm using a microplate reader. The total phenolic acid content was expressed as gallic acid equivalents (mg GAE/g).

2.2.2. Determination of the total flavonoid content

The total flavonoid content was determined using a method described by Tambe and Bhambar (2014). Briefly, methanolic extracts (50 µl; 1 mg/mL) were added to 950 µL of sterile distilled water in separate glass test tubes. Methanol: HCl (2.5 mL; 5:1 v/v) and 2.5 mL of vanillin reagent (1%, w/v) were also added to the reaction mixture, which was incubated in a water bath at 30 °C for 30 minutes. Catechin was used as a positive control, while a reaction mixture containing 80% aqueous methanol (v/v) was used as a negative control. The samples were then transferred to a 96-well plate, and the absorbance was read at 500 nm using a microplate reader. The total flavonoid content was expressed as catechin equivalents (mg CE/g).

2.3. Antioxidant activity assay

2.3.1. DPPH (2, 2-diphenyl-1-picryhydrazyl) radical scavenging activity

The ability of plant extracts to reduce free radicals was determined using the DPPH radical scavenging assay as described by Karioti et al. (2004). Methanolic extracts (30 µL; 10 mg/mL) were serially diluted by two-folds with 80% aqueous methanol (v/v). Methanol (1.47 mL) and a methanolic DPPH solution (1.5 mL; 0.1mM) were added to the extract mixture in a glass test tube. The reaction was performed under low-light conditions, and the reaction mixture was incubated at room temperature (25°C) for 30 minutes.

L-Ascorbic acid was used as a positive control, and the reaction mixture without any plant extract served as a negative control. A microplate reader was used to measure the absorbance of the reaction mixture at 517 nm. The discoloration of the purple-colored DPPH working solution by the free radical scavenging activity (RSA) of plant extracts was calculated according to Equation (1):

$$\%\text{RSA} = 1 - \left(\frac{A_E}{A_D}\right) \times 100\% \quad (1)$$

where A_E is the absorbance of the reaction mixture containing the sample extract/standard antioxidant and A_D is the absorbance of the DPPH solution alone. The %RSA was plotted against the plant extract concentration, and the IC_{50} was determined from the normalized logarithmic regression curve.

2.3.2. Ferric reducing antioxidant power (FRAP) assay

The ferric-reducing potential of the plant extracts was determined using the FRAP method as described by Lim et al. (2009). Plant extracts (30 µL; 10 mg/mL) were serially diluted with 30 µL of methanol down the 96-well microtiter plate. Potassium phosphate buffer (30 µL; 0.2M; pH 7.2) and potassium ferricyanide (30 µL; 1%, w/v) were later added to each well. The reaction mixture was protected from light, and the plate was wrapped with aluminum foil and incubated at 50°C for 20 minutes. Trichloroacetic acid (TCA) (30 µL; 10%, w/v), 80 µL distilled water, and FeCL3 (30 µL; 0.1%, w/v) were added to the reaction mixtures, which were then further incubated for 30 minutes at room temperature in the dark. L-Ascorbic acid served as the antioxidant positive control, and methanol served as the negative control. The microplate reader was used to measure the absorbance at 630 nm. A line graph of FRAP percentage inhibition versus plant extract concentration was plotted, and the IC_{50} was determined from the normalized logarithmic regression curve.

2.3.3. Hydrogen peroxide (H_2O_2) reducing assay

The hydrogen peroxide scavenging potential of plant extracts was evaluated using the H_2O_2 method as described by Jayaprakasha et al. (2004). Methanolic extracts (250 µL; 10 mg/mL) were serially diluted with distilled water. Phosphate buffer (1 mL; 50 mM; pH 7.4) and H_2O_2 solution (1.5ml; 40mM) were added to each test tube. The reaction mixture was vortexed and then incubated at room temperature for 10 minutes. Quercetin was used as the positive control, and the reaction mixture without any plant extract served as a negative control. Absorbance was measured at 560 nm against blank solutions containing plant extracts in phosphate buffer saline without H_2O_2. A line graph of H_2O_2 percentage inhibition versus plant extract concentration was plotted, and the IC_{50} was determined from the normalized logarithmic regression curve.

2.4. Determination of volatile phytoconstituents

2.4.1. Detection and identification using GC-MS analysis

The detection and identification of volatile compounds test was performed as described by Gololo et al. (2016). Briefly, prepared GC-MS analytical vials with extracts of *E. globulus*, *S. molle*, and *S. lancea* were analyzed using a SHIMADZU QP2010 SE GC-MS with an inert cap 5MS/SIL, silica capillary column (30 mm × 0.25 mm ID × 1 µm df, composed of 100% dimethyl-polysiloxane). For detection, an electron-ionization system with an ionization energy of 70 eV was used. The carrier gas used was helium (99.99%) at a constant flow rate of 1 mL/min, with an injection volume of 2 µL, an injector temperature of 290°C, and an ion-source temperature of 230°C. The oven temperature was set to 50°C (isothermal for 1 min), then increased at 20°C/min to 180°C (isothermal for 5 minutes), then to 240°C at 20°C/min, and finally to 280°C (isothermal for 5 minutes). The mass spectra were taken at 70eV; scan interval of 0.3 sec and fragments from 50 to 700 m/z. The total GC running time was determined thereafter, and the relative % amounts of each component were calculated by comparing their average peak areas to the total area. GC-MS Solutions version 2.6 software was adopted to handle mass spectra and chromatograms. Identification of unknown compounds was compared with components in the National Institute of Standards and Technology (NIST08) library, with hits of 80% or higher regarded as a positive match.

2.5. In vitro antiviral activity studies

2.5.1. Neuraminidase activity assay

The antiviral (H1N1) potential of the selected plant extracts was performed using the Amplex™ Red neuraminidase assay kit (ThermoFisher Scientific, Waltham, MA USA) as per manufacturer's instructions. Briefly, hexane, acetone, and methanol extracts (50 µL; 1 mg/mL) were added to the first well containing 50 µL reaction buffer and serially diluted down the microtiter plate. A volume of 50 µL of a reaction mixture prepared by adding Amplex™ red reagent (50 µL; 100 µM), horseradish peroxidase (10 µL; 0.2 units/mL), galactose oxidase (100 µL; 4 units/mL), fetuin (250 µL; 500 µg/mL), and 4.59 mL 1× reaction buffer was added to each well. Neuraminidase (1–5 U/mL) and H_2O_2 (10 µM) served as the positive control, and reaction buffer alone served as the negative control. The plate was protected from light by wrapping

with aluminum foil and incubated at 37 °C for 30 minutes. In the presence of horseradish peroxidase, H_2O_2 interacts with the Amplex™ Red reagent in a 1:1 ratio to produce the red-fluorescent oxidation product, resorufin. A microplate reader was used to measure absorbance at 560 nm, and results were recorded. The IC_{50} was determined from the normalized logarithmic regression curve of the neuraminidase percentage inhibition.

2.5.2. Papain-like protease activity assay

The antiviral (SARS-CoV-2) potential of the selected plant extracts was assessed using the papain-like protease assay kit according to the manufacturer's instructions (BPS Bioscience, San Diego, CA 92121). Briefly, a reaction mixture was prepared by adding hexane extracts (10 µL; 1 mg/mL) to the first well containing 10µl PL^{pro} assay buffer and serially diluted down the microtiter plate. A PL^{pro} enzyme solution (30 µL; 0.5 ng/µL) was added to each well, and the reaction mixture was pre-incubated at 37 °C for 30 minutes. The reaction was initiated by adding the substrate solution (10 µL; 125 µM) to each well to make a final volume of 50 µL, and the plate was sealed with a plate sealer and further incubated at 37 °C for 60 minutes. A plate reader was used to measure fluorescence intensity at an excitation of 360 nm and emission of 460 nm.

2.6. In silico binding efficiency analysis of potential bioactive constituents

Following GC-MS analysis of extracts to determine their chemical constituents and subsequent in vitro assessment, molecular modeling and molecular dynamics calculations were used to predict bioactive molecules. All in silico studies were conducted through the Maestro 13.6 program (Schrodinger Inc, USA). We strategically selected the ligands based on the in vitro biological activity of each plant extract. The positive controls used in the in vitro screening were also included. The protein targets used in this study were obtained from Protein Data Bank (PDB). These included the closely related SARS-CoV-2 proteases that work in complementarity (PDB: 7CMD and 7MB1) in the proteolytic processing of SARS-Cov-2 polyproteins during replication (Narayanan et al., 2022), and neuraminidase target 1BJI, the only crystal structure of influenza neuraminidase in the PDB at the time this study was executed. The initial molecular modeling was conducted using the stringent extra-precision docking protocol (Rants'o et al., 2022a, 2022b). The pre-docking steps included ligand preparation, receptor optimization and minimization, and binding site identification using the original ligands complexed with the receptors. Docking used the prepared ligands and receptors under the extra precision protocol (Narayanan et al., 2022). The best candidates from this first phase were selected based on their docking scores and binding conformation, relative to the positive control. These were subjected to further binding accuracy and stability testing using advanced techniques, including molecular mechanics and molecular dynamics calculations (Antony and Vijayan, 2021). REDOCKING?

To assess the binding accuracy, the molecular mechanics-generalized born surface area (MM-GBSA) redocking study was performed (Massova and Kollman, 2000). MM-GBSA is known for its superior performance in reliably predicting binding affinities and ligand poses (Tuffery and Derreumaux, 2012; Rants'o et al., 2022a). In the Schrödinger Prime MM-GBSA platform, the initial extra-precision complexes were subjected to the OPLS4 force field in the VGSB solvation model. To allow for flexible binding, the distance between ligand and receptor was increased from 0 Å to 5 Å (Rants'o et al., 2022a). The ligand-receptor flexibility, along with the implicit solvent model, mimics normal physiology and increases binding accuracy (Rants'o et al., 2022a).

To perform molecular dynamics, a simulation system containing a 0.15 M NaCl and buffer solution in the TIP3P solvent model was developed using the Desmond System Builder (van der Westhuizen et al., 2022). This system was generated in an orthorhombic box placed 10 Å from the protein surface and subsequently minimized to ~35,000 atoms (7MB1) and ~45,000 atoms (1BJI) using the OPLS4 force field. This system was then used to initiate molecular dynamics simulation for the duration of 100 ns. Parameters included the standard relaxation protocol, the isothermal-isobaric factor of 310K and 1.103 bar, as well as the default integrator size and Coulombic cutoff. Results were analyzed on the Desmond simulation interaction diagram platform (van der Westhuizen et al., 2022).

2.7. Statistical analysis

The differences in results amongst plants were determined using one-way analysis of variance (ANOVA) in the IBM Statistical Package for the Social Sciences (SPSS). Means were separated and compared using a student t-test, and differences between means were considered significant at $p < 0.05$. GC-MS Solutions version 2.6 software was adopted to handle mass spectra and chromatograms. Tentative identification of unknown compounds was based on GC-MS mass spectra obtained using the National Institute of Standards and Technology (NIST08) library. The molecular docking system was subsequently minimized to approximately 35,000 atoms using the OPLS4 force. This system was then used to initiate an MD simulation for 100 ns. Parameters included the

standard relaxation protocol, the isothermal-isobaric factor of 310K and 1.103 bar, respectively, the default integrator size, and the Coulombic cutoff.

3. RESULTS AND DISCUSSION

3.1. Phytochemical content analysis

The total phenolic and total flavonoid contents of three medicinal plants, namely *E. globulus*, *S. molle*, and *S. lancea*, were quantitatively determined, and the results are presented in Table 2. Plant extract of *S. molle* expressed a level of 82.61 ± 8.57 mg GAE/g which was the lowest when compared to the other plant extracts. *Eucalyptus globulus* and *S. lancea* expressed total phenolic content of 156.40 ± 8.53 mg GAE/g and 154.54 ± 12.26 mg GAE/g, respectively. The total flavonoid and phenolic content for *S. molle* was significantly lower when compared to those of *E. globulus* and *S. lancea*. different for *E. globulus*, *S. molle* and *S. lancea* with mean values of 26.03 ± 2.77 mg CE/g, 9.91 ± 1.72 mg CE/g and 35.49 ± 2.00 mg CE/g, respectively. Extracts of *S. lancea* showed the highest presence of flavonoids than *E. globulus*, followed by *S. molle* having the least levels of flavonoids.

All three selected plants emit an aroma that suggests the presence of aromatic compounds (Almas et al., 2021; Bvenura and Kambizi, 2022; Vambe et al., 2018). Aromatic compounds are organic hydrocarbons characterized by a stable ring structure with a specific arrangement of pi electrons in a conjugated system (Lin et al., 2016). Phenols are a class of organic compounds that contain a hydroxyl group, which is responsible for their reducing ability. Aromatic phenols are characterized by having the hydroxyl group attached to an aromatic ring. While some non-aromatic phenols such as aliphatic compounds are bonded to a non-aromatic carbon chain (Bvenura and Kambizi, 2022). The substituents of the ring structure are responsible for the compound's activity as well as size (Shoker et al., 2023). The total phenolic content assay considers the overall measure of phenolic compounds, from simple to complex, which may account for the high concentration observed in all three plant samples (Tambe and Bhambar, 2014). Phenolic compounds such as rutin, quercetin, myricetin, and luteoline have been reported to be present in leaves of *E. globulus,* accounting for its high phenolic content (Dezsi et al., 2015). Rutin has been reported to have antioxidant properties (Rahmani et al., 2023). Additionally, rutin inhibits the binding and entry of SARS-CoV-2 and co-infecting viruses into host cells by blocking viral attachment to cell-surface receptors (Mazik, 2022).

Research suggests that myricetin may inhibit influenza virus replication and alleviate respiratory conditions by reducing inflammation. The leaves of *S. lancea* have recently been reported to contain quercetin, kaempferol, gallic acid, and catechins (Koki et al., 2022). Proanthocyanidins hinder the early stage of viral attachment by attaching to viral hemagglutinin (HA) proteins (Morimoto et al., 2022). Furthermore, proanthocyanidins can inhibit the binding of influenza virus particles to host cell-surface receptors, specifically sialic acid residues on respiratory epithelial cells (Morimoto et al., 2022). Therefore, the presence of phenols suggests that all three plant extracts may have the potential to exhibit antiviral activity (Montenegro-Landívar et al., 2021).

Extracts of *S. lancea showed the highest concentrations of flavonoids, followed by E. globulus and S. molle*. Flavonoids are a subclass of phenolic compounds that are distinguished by a 15-carbon structure comprising two aromatic rings (A and B) that are joined by a three-carbon bridge (Awouafack et al., 2017). Medicinal plants are known to contain several classes of flavonoids, including quercetin, kaempferol, and myricetin. For example, kaempferol has been reported to activate an immune system response, aiding the body in warding off diseases (Dong et al., 2014). Kaempferol additionally regulates cytokine synthesis by inhibiting the release of pro-inflammatory cytokines and enhancing the release of anti-inflammatory cytokines (Dong et al., 2014). Furthermore, quercetin has been reported to inhibit the replication of several viruses, including the hepatitis B, herpes simplex, and influenza viruses (Mehrbod et al., 2020).

The replication-inhibitory potential of quercetin against influenza virus, for instance, was due to its ability to block neuraminidase activity (Wu et al., 2015). The antiviral activity of quercetin was further attributed to its antioxidant properties in mitigating the oxidative stress induced by viral infections, thereby limiting viral replication (Mehrbod et al., 2020). The abundance of flavonoids in medicinal plants is beneficial for treating viral infections, especially when current antiviral remedies have been reported to be ineffective. Myricetin has been shown to have anti-inflammatory

Table 2
Results for the total phenolic and total flavonoid content of selected medicinal plants commonly used against colds and flu.

Medicinal plant	Total phenolic content (mg GAE/g)	Total flavonoid content (mg CE/g)
Eucalyptus globulus	156.40 ± 8.53	26.03±2.77
Schinus molle	**82.61 ± 8.57****	**9.91±1.72****
Searsia lancea	154.54 ± 12.26	35.49±2.00

Results are presented as mean values ± standard deviation; **Means significant difference with a $p < 0.0001$.

properties, helping reduce inflammation and tissue damage caused by viral infections (Sang et al., 2021).

3.2. Antioxidant activity assays

3.2.1. DPPH radical scavenging activity assay

The % RSA inhibition of the selected three plants is presented for *E. globulus* (Figure 1A), *S. molle* (Figure 1B), *S. lancea* (Figure 1C), and ascorbic acid (Figure 1D). The graphs of % RSA inhibition exhibit a sigmoidal pattern characteristic of activity-based studies (Suriyatem et al., 2017). The linear regression of the logarithmic plots was used to calculate IC_{50} values (Sebaugh, 2011).

The DPPH assay primarily measures the ability of the samples to act as a free radical scavenger whereby antioxidants react with 2,2-diphenyl-β-picrylhydrazyl (DPPH) to reduce it to 2,2-diphenyl-β-picrylhydrazine (DPPH-H), indicating the scavenging potential of the antioxidant compound or extract. Investigating the antioxidant potential, the tested plant extracts induced a visible discoloration of the purple DPPH free radical, transforming it into the colorless DPPH-H. Methanolic extracts of *E. globulus*, *S. molle,* and *S. lancea* exhibited significant radical scavenging potential with IC_{50} values of 20.098 ± 0.96, 28.790 ± 1.12, and 17.747 ± 0.37 µg/mL, respectively (Figure 1). The radical scavenging potential of all three plant extracts was significantly lower than that of the positive control which was 5.327 ± 0.19 µg/mL.

The chemical composition of the selected medicinal plants is rich in antioxidants that effectively scavenge free radicals. Viral infections often trigger an inflammatory response and induce the production of free radicals as a natural host's immune system defense mechanism. This can result in excessive production of oxidants, ultimately leading to oxidative damage (Çalişkan and Çalişkan, 2021). The presence of secondary metabolites with radical scavenging properties can provide additional support to the body's defense system against oxidative damage (Pizzino et al., 2017).

3.2.2. Ferric reducing antioxidant potential assay

The % inhibition of ferric reduction of the selected three plants is presented for *E. globulus* (Figure 2A), *S. molle* (Figure 2B), *S. lancea* (Figure 2C), and ascorbic acid (Figure 2D). The graphs of % inhibition of ferric reduction show a sigmoidal

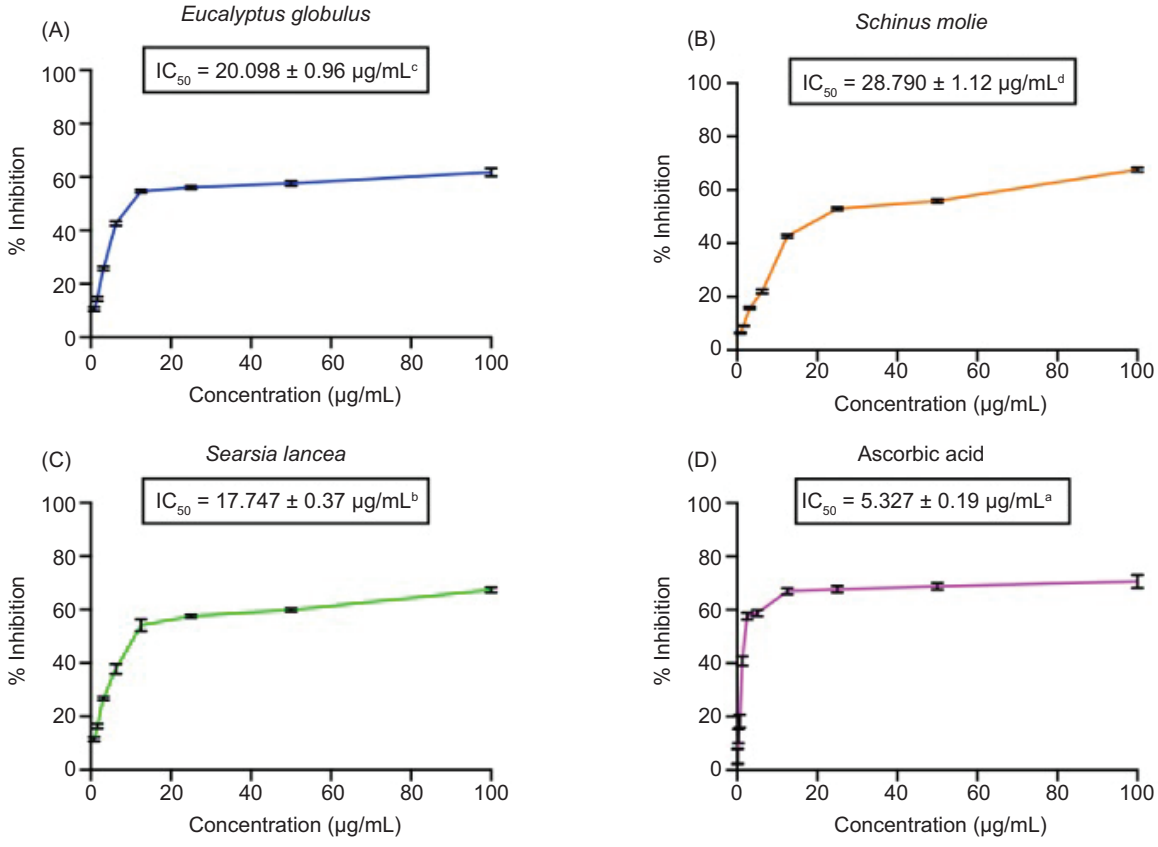

Figure 1. Diagrammatic illustration of the % RSA and IC_{50} values of plants commonly used against colds and flu based on DPPH assay. IC_{50} results are presented in mean values ± standard deviation; Alphabetical letters indicate $p < 0.05$.

pattern characteristic of activity-based studies (Suriyatem et al., 2017). The linear regression of the logarithmic plots was used to calculate IC_{50} values (Sebaugh, 2011).

The FRAP assay primarily measures the sample's ability to reduce ferric ion (Fe^{3+}) to ferrous ion (Fe^{2+}), and the reduction capacity is directly proportional to the antioxidant activity of the sample (González-Palma et al., 2016). Methanolic extracts of *E. globulus*, *S. molle,* and *S. lancea* exhibited significant radical scavenging potential with IC_{50} values of 26.64 ± 1.266, 71.90 ± 2.805, and 45.31 ± 1.222 µg/mL, respectively (Figure 2). The ferric-reducing antioxidant potential of all three plant extracts was significantly lower than that of the positive control, which was 5.77 ± 0.333 µg/mL. This validates the potential antioxidant activity of all three plant samples to reduce ferric ions.

There is biological variability within sample populations, leading to differences in chemical composition and antioxidant potential among samples (Rajurkar and Hande, 2011). Oxidative stress, which can be reduced by antioxidants, can weaken the immune system, and make individuals more susceptible to viral infections (Fernandes et al., 2016). Fenton reactions, which produce hydroxyl radicals when hydrogen peroxide and ferrous iron are present, play a crucial role in the immune system's response to viral infections (Schallreuter et al., 2012). The production of these hydroxyl radicals can trigger oxidative stress, stimulating the production of antiviral proteins and cytokines, which ultimately enhance the immune system's ability to combat viruses (Wu, 2020). Additionally, high concentrations of hydroxyl radicals directly obstruct viral particles, hindering their replication and spread (Molteni et al., 2014). Fenton reactions can also promote the production of antioxidant enzymes that protect cells from oxidative stress (Molteni et al., 2014). The antioxidant activity expressed by the above medicinal plants can help mitigate the detrimental effects of oxidative stress (Chaves et al., 2020). Due to the hydroxyl group, phenols and flavonoids can act as reducing agents (Awouafack et al., 2017).

3.2.3. Hydrogen peroxide (H_2O_2) scavenging activity assay

The H_2O_2 % inhibition of the selected three plants is presented for *E. globulus* (Figure 3A), *S. molle* (Figure 3B), *S. lancea* (Figure 3C), and quercetin (Figure 3D). The graphs

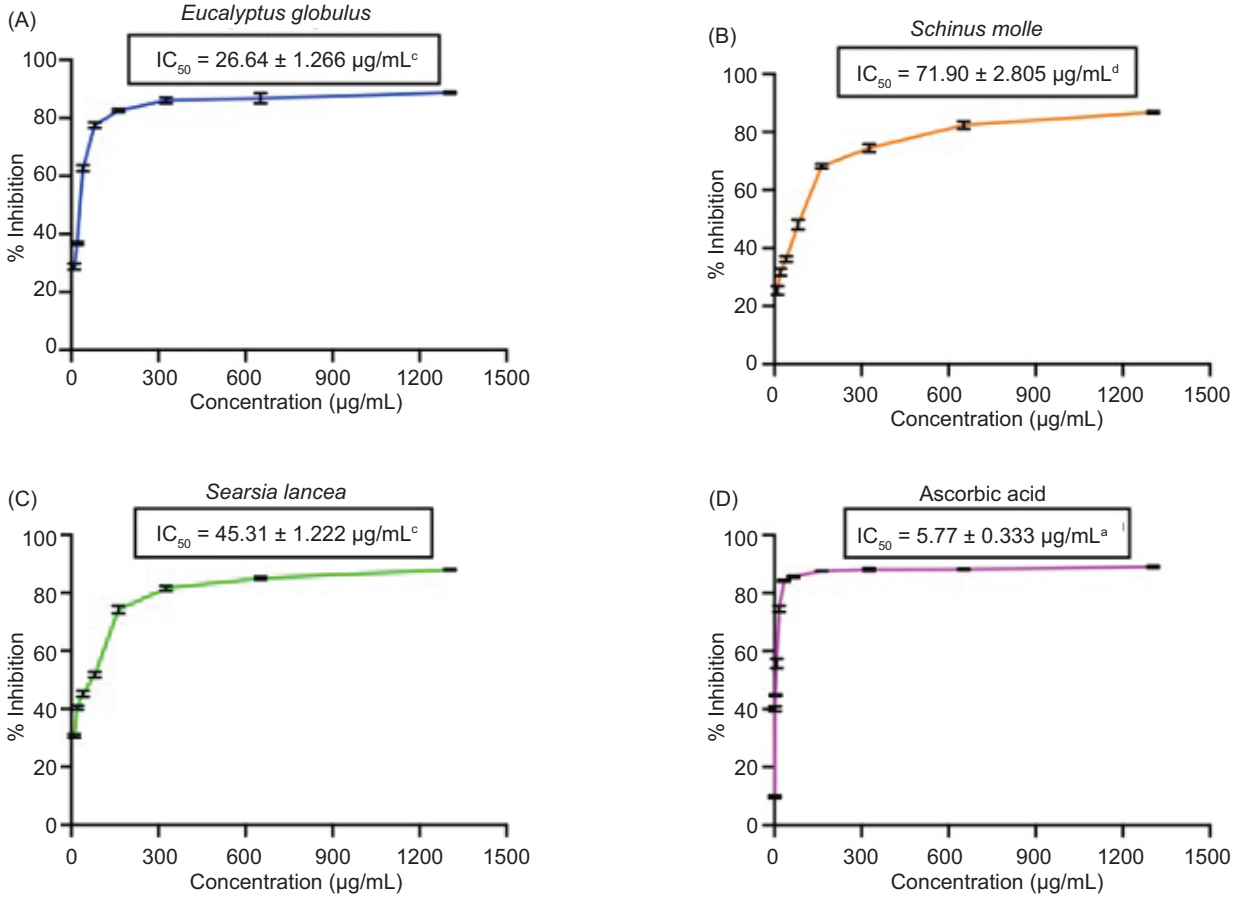

Figure 2. Diagrammatic illustration of the % RSA and IC_{50} values of plants commonly used against colds and flu based on FRAP assay. IC_{50} results are presented in mean values ± standard deviation; Alphabetical letters indicate $p < 0.05$.

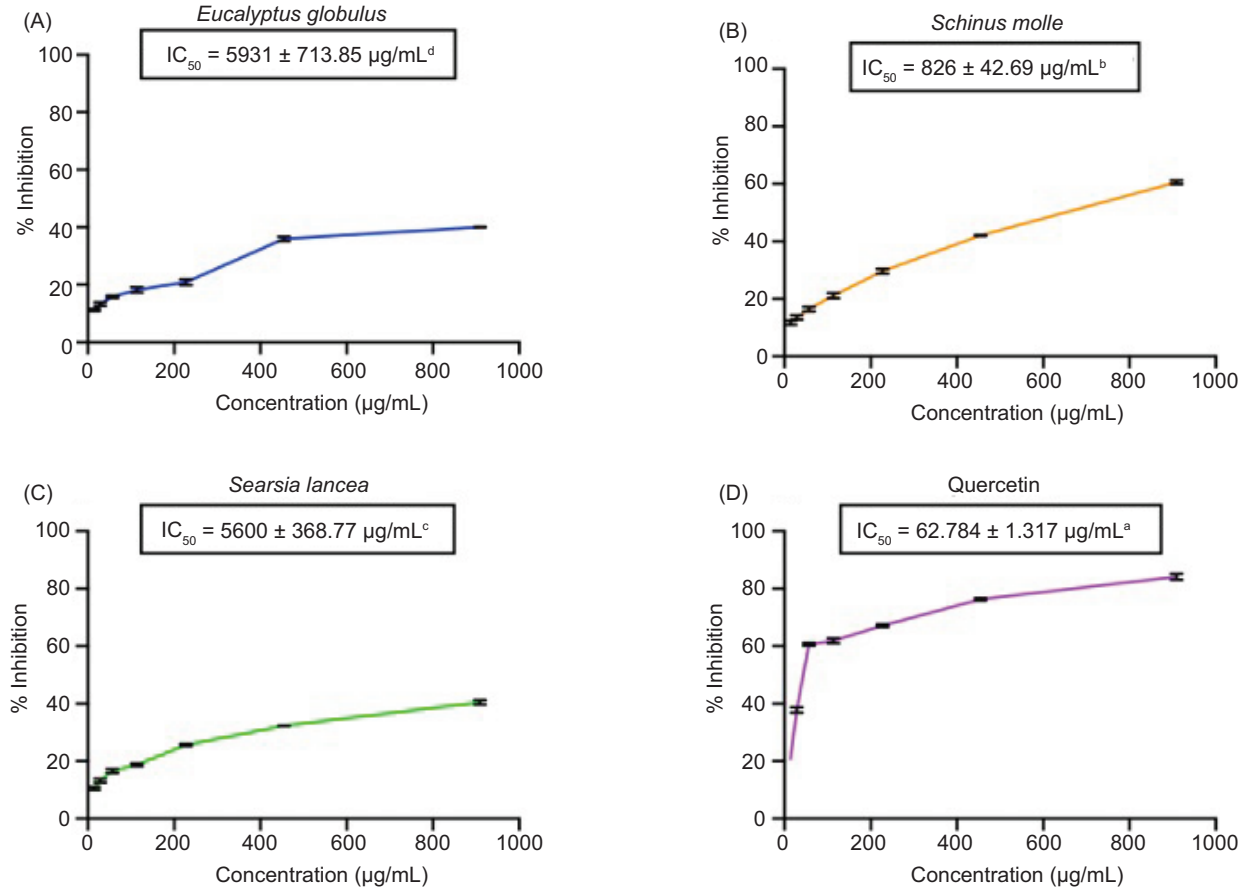

Figure 3. Diagrammatic illustration of the % RSA and IC_{50} values of plants commonly used against colds and flu based on H_2O_2 assay. IC_{50} results are presented in mean values ± standard deviation; Alphabetical letters indicate $p < 0.05$.

for the % inhibition of peroxide scavenger portray a sigmoidal pattern characteristic of activity-based studies (Suriyatem et al., 2017). The linear regression of the logarithmic plots was used to calculate IC_{50} values (Sebaugh, 2011). The H_2O_2 activity assay primarily measures a sample's ability to act as a peroxide scavenger (Fernando and Soysa, 2015). Methanolic extracts of *S. molle* exhibited notable peroxide scavenging potential with an IC_{50} value of 826 ± 42.69 µg/mL (Figure 3).

Even though the antioxidant activity of the plant extracts against H2O2 is lower than the DPPH and FRAP results, *S. molle* demonstrated better inhibitory potential in the H_2O_2 assay. The current concentrations of *E. globulus* and *S. lancea* samples cannot effectively scavenge hydrogen peroxide, a reactive oxygen species that can cause damage to cells and tissues (Özen and Kinalioğlu, 2008). With an increase in the concentration of plant samples, desirable results can be achieved, and hydrogen peroxide-like oxidative species can be reduced (Hyland et al., 2012). However, increasing the concentration beyond the current working concentration will be toxic to host cells rather than therapeutic (Ramulondi et al., 2019). Some studies have reported that hydrogen peroxide can augment the antiviral capabilities of immune cells, particularly macrophages and neutrophils (Dumas and Knaus, 2021). This is achieved by stimulating the production of antiviral cytokines, leading to viral clearance (Dumas and Knaus, 2021). Hydrogen peroxide scavenging activity of *S. molle* can indirectly enhance the immune cells' antiviral defense systems by regulating hydrogen peroxide levels and enhancing their antiviral effects (Caruso et al., 2020). The assay results did not demonstrate desirable scavenging of hydrogen peroxide by *E. globulus* and *S. lancea* plant extracts at working concentrations.

3.3. Determination of volatile phytoconstituents

3.3.1. Detection and identification using GC-MS analysis

The presence of bioactive chemicals in the extract of *E. globulus* leaves was detected using GC-MS analysis, and their chemical composition was recorded in Table 3. The results include hydrocarbons, fatty acids, alcohols, aldehydes, and esters. The leaves of *E. globulus* possess a notable quantity

Table 3
Chemical composition of the hexane extract of *Eucalyptus globulus* leaves.

Functional group	Name	Retention times	Molecular weight	Molecular formula	Peak area %
Alcohols	Globulol	8.665	222	$C_{15}H_{26}O$	1.42
	Ledol	8.680	222	$C_{15}H_{26}O$	1.11
	trans-2-Undecen-1-ol	9.407	170	$C_{11}H_{22}O$	1.44
	2-Decen-1-ol, (E)-	4.420	156	$C_{10}H_{20}O$	1.72
	Cyclohexanol, 2-methyl-5-(1-methylethenyl)-	4.160	154	$C_{10}H_{18}O$	2.02
	n-Tetracosanol-1	8.500	354	$C_{24}H_{50}O$	1.71
	1-Octanol, 2-butyl-	4.690	186	$C_{12}H_{26}O$	2.97
Aldehydes	2-Decenal, (E)-	4.180	154	$C_{10}H_{18}O$	1.80
	2-Tridecenal, (E)-	5.035	196	$C_{13}H_{24}O$	1.81
	9-Octadecenal	5.210	266	$C_{18}H_{34}O$	1.43
Alkanes	Nonane	3.020	128	$C_{9}H_{20}$	3.21
	Decane, 2-methyl-	4.400	156	$C_{11}H_{24}$	3.28
	Undecane, 2-methyl-	4.710	170	$C_{12}H_{26}$	0.06
	Tridecane	4.695	184	$C_{13}H_{28}$	37.44
	Heptadecane	16.200	240	$C_{17}H_{36}$	9.36
	Decane, 2,3,5,8-tetramethyl-	8.540	198	$C_{14}H_{30}$	3.53
Alkenes	1-Pentadecene, 2-methyl-	4.320	224	$C_{16}H_{32}$	1.66
	1,12-Tridecadiene	5.030	180	$C_{13}H_{24}$	1.65
	1-Pentadecene, 2-methyl-	4.320	224	$C_{16}H_{32}$	1.73
	1-Nonene, 4,6,8-trimethyl-	5.230	168	$C_{12}H_{24}$	2.20
	Naphthalene, decahydro-2-methyl-	4.895	152	$C_{11}H_{20}$	1.65
Esters	Pentanoic acid, 10-undecenyl ester	5.455	254	$C_{16}H_{30}O_{2}$	1.45
Fatty acids	Pentadecanoic acid	14.350	242	$C_{15}H_{30}O_{2}$	1.37
Terpenes	Camphene	6.625	136	$C_{10}H_{16}$	1.47
	cis-.alpha.-Bisabolene	7.430	204	$C_{15}H_{24}$	1.28
	alpha.-Caryophyllene	7.84	204	$C_{15}H_{24}$	1.34
	alpha.-Pinene	6.635	136	$C_{10}H_{16}$	1.48
	Limonene	4.145	136	$C_{10}H_{16}$	8.42

of hydrocarbons, which are observed to constitute the largest percentage of peak area. These hydrocarbons include alkanes, alkenes, and terpenes. Tridecane, Heptadecane, and limonene had the largest peak % with a yield of 37.44%, 9.36%, and 8.42%, respectively.

Heptadecane is a hydrophobic organic compound which is an essential volatile oil of plants such as *Opuntia littoralis*. Little has been reported on the antiviral properties of heptadecane, however, it has been reported to exert anti-inflammatory effect in aged kidney tissues (Kim et al., 2013). Limonene, α-pinene, and some other hydrocarbons found in *E. globulus* have been reported to exhibit immunomodulatory and antiviral properties (Astani and Schnitzler, 2014; Himed et al., 2019). Medicinal plants containing limonene as a major constituent have been reported to possess anti-inflammatory and analgesic activities (Fadilah et al., 2022). Limonene has been studied in COVID-19 research due to its lack of cytotoxicity, its low irritancy when diluted, and its favorable pharmacokinetic characteristics (Corrêa et al., 2023). Limonene is a cyclic monoterpene, an essential oil found in medicinal plants and citrus fruits (Meeran et al., 2021). Limonene has been reported to inhibit viral replication of the influenza H1N1 virus through direct action on the virus (Setzer, 2016). Furthermore, limonene has been proposed to inhibit viral infection by blocking the ACE-2 and TMPRSS receptors (Meeran et al., 2021). Caryophyllene, one of the detected terpenes, has shown to protect the host from the risk factors, prevent the entry of the virus, and ameliorate organ damage and the pathological manifestation of SARS-CoV-2 on the different organ systems (Jha et al., 2021). This is achieved through the mediation of the activation of Cannabinoid type 2 receptors (Jha et al., 2021).

Most of the reported antiviral activity emanates from the presence of terpenes, which, unlike heptadecane and tridecane, are present in quantities less than 5%. Through fractional distillation, terpenes can be separated from other compounds in plant samples and enriched due to their low boiling point (Frolova et al., 2019). By enriching these terpenes, the yield would be lowered; however, the antiviral activity would be maximized. Main compounds such as 1,8-cineole may be found in polar extracts, including methanol (Jerbi et al., 2017). However, this study only focused on the hexane extracts due to their polarity. The antiviral properties of *E. globulus* can be attributed to the presence of bioactive compounds. The biological activities exhibited by the essential oil of *E. globulus* emphasize the potential efficacy of this medicinal plant in healthcare against respiratory infections, including H1N1 and SARS-CoV-2.

The presence of bioactive chemicals in the hexane extract of *S. molle* leaves was detected using GC-MS analysis and their chemical composition was recorded in Table 4. The results include hydrocarbons, carboxylic acids, alcohols,

Table 4
Chemical composition of the hexane extract of *Schinus molle* leaves.

Functional group	Name	Retention times	Molecular weight	Molecular formula	Peak area %
Alcohols	1-Heptanol, 2-propyl-	5.190	158	$C_{10}H_{22}O$	1.05
	1-Pentanol, 4-methyl-2-propyl-	4.385	144	$C_9H_{20}O$	0.9
	1-Hexacosanol	4.440	382	$C_{26}H_{54}O$	0.93
	Bi-cyclo[3.1.0]hexan-3-ol, 4-methyl-1-(1-methylethyl)-	8.065	154	$C_{10}H_{18}O$	7.39
	2,6,10,14-Hexadecatetraen-1-ol, 3,7,11,15-tetramethyl-, acetate, (E,E,E)	8.540	332	$C_{22}H_{36}O_2$	5.17
	n-Tetracosanol-1	4.320	354	$C_{24}H_{50}O$	0.91
	3,6-Octadien-1-ol, 3,7-dimethyl-, (Z)-	8.105	154	$C_{10}H_{18}O$	5.62
	Cyclohexanemethanol, 4-ethenyl-.alpha.,.alpha.,4-trimethyl-3-(1-methylethenyl)-, [1R-(1.alpha.,3.alpha.,4.beta.)]-	8.040	222	$C_{15}H_{26}O$	0.8
	2-Decen-1-ol, (E)-	4.420	156	$C_{10}H_{20}O$	0.86
	trans-2-Undecen-1-ol	4.795	170	$C_{11}H_{22}O$	0.97
Aldehydes	Decanal	4.410	156	$C_{10}H_{20}O$	0.83
	4,8,12-Tetradecatrienal, 5,9,13-trimethyl-	20.130	248	$C_{17}H_{28}O$	2.49
Alkanes	Decane, 2-methyl-	4.395	156	$C_{11}H_{24}$	1.74
	Tridecane	8.575	184	$C_{13}H_{28}$	27.94
	Pentadecane	5.530	212	$C_{15}H_{32}$	14.01
	Hexadecane	11.150	226	$C_{16}H_{34}$	3.44
	Eicosane	11.115	282	$C_{20}H_{42}$	1.68
Alkenes	6-Dodecene, (Z)-	4.650	168	$C_{12}H_{24}$	0.84
	1,12-Tridecadiene	5.030	180	$C_{13}H_{24}$	0.92
	1,9-Tetradecadiene	5.450	194	$C_{14}H_{26}$	0.86
	1-Decene, 4-methyl-	5.625	154	$C_{11}H_{22}$	2.07
	1,6-Cyclodecadiene, 1-methyl-5-methylene-8-(1-methylethyl)-, [s-(E,E)]-	7.735	204	$C_{15}H_{24}$	0.7
	2,6,10,14,18,22-Tetracosahexaene, 2,6,10,15,19,23-hexamethyl-, (all-E)-	20.130	410	$C_{30}H_{50}$	2.42
Alkyne	1-Undecyne	4.890	152	$C_{11}H_{20}$	0.96
Carboxylic acid	n-Hexadecanoic acid	14.380	256	$C_{16}H_{32}O_2$	0.93
	9,12,15-Octadecatrienoic acid, (Z,Z,Z)-	15.995	278	$C_{18}H_{30}O_2$	0.58
Cyclic Ether	5,10-Dioxatricyclo[7.1.0.0(4,6)]decane	4.160	140	$C_8H_{12}O_2$	0.91
Cycloalkane	Cyclopentane, 1-methyl-3-(2-methylpropyl)-	4.595	140	$C_{10}H_{20}$	0.89
Epoxide	Oxirane, dodecyl-	4.415	212	$C_{14}H_{28}O$	0.89
Ester	Pentanoic acid, 10-undecenyl ester	5.445	254	$C_{16}H_{30}O_2$	0.81
Ether	Heptane, 3-[(ethenyloxy)methyl]-	4.035	156	$C_{10}H_{20}O$	0.97
	Isooctane, (ethenyloxy)-	4.720	156	$C_{10}H_{20}O$	3.21
Ketone	4-Heptanone, 3-methyl-	3.010	128	$C_8H_{16}O$	1.27
Terpene	Limonene	4.140	136	$C_{10}H_{16}$	4.05

aldehydes, ethers, epoxides, ketones, polyenes, and esters. The leaves of *S. molle* possess a notable quantity of hydrocarbons, which are observed to constitute the largest percentage of peak area. These hydrocarbons include alkanes, alkenes, alkynes, and terpenes. Tridecane; pentadecane; Bicyclo[3.1.0]hexan-3-ol,4-methyl-1-(1-methylethyl)-; 3,6-Octadien-1-ol,3,7-dimethyl-(Z)- and 2,6,10,14-Hexadecatetraen-1-ol,3,7,11,15-tetramethyl-acetate,(E,E,E)- with peak % of 27.94%, 14.01%, 7.39%, 5.62%, and 5.17% are the compounds with the highest peak area.

Tridecane and pentadecane are both colorless alkanes with 13 carbon atoms and 15 carbon atoms in their structure, respectively. Tridecane forms part of various solvents and fuels; however, like pentadecane, no specific antiviral activity has been reported on their structures (Touazi et al., 2024). Bicyclo[3.1.0]hexan-3-ol,4-methyl-1-(1-methylethyl)-; 3,6-Octadien-1-ol,3,7-dimethyl-(Z)- and 2,6,10,14-Hexadecatetraen-1-ol,3,7,11,15-tetramethyl-, acetate,(E,E,E)- are alcohols constituting the third, fourth, and fifth most major peak areas in the chemical composition of *S. molle* leaf extracts. The antiviral activity of the compounds to combat H1N1 and SARS-CoV-2 infections is little to inadequate. The bioactive compounds, such as limonene, found in *S. molle* possess antiviral and anti-inflammatory properties as well. The mechanism and properties of limonene were previously described under E. globulus since the compound is present in both plant samples. Respiratory infections such as colds and flu, as well as SARS CoV-2, present a risk to public health; however, chemical compositions, including limonene and other compounds, can potentially aid in the alleviation of these respiratory symptoms. Studies have been conducted that report on the ability of essential oils to regulate the immune responses and limit extreme inflammatory responses, which can result in severe respiratory symptoms (Jha et al., 2021). *Schinus molle* has been medicinally used for treating colds and flu symptoms through inhaling steam from boiled leaves (Magwede and Van Wyk, 2016). The presence of volatile constituents accounts for this method of administration in South African homes.

The presence of bioactive chemicals in the hexane extract of *S. lancea* leaves was detected using GC-MS analysis, and their chemical composition was recorded in Table 5. The results include hydrocarbons, alcohols, aldehydes, epoxides, ketones, siloxanes, and esters. The leaves of *S. lancea* possess a notable quantity of hydrocarbons, which are observed to constitute the largest percentage of peak area. These hydrocarbons include alkanes, alkenes, alkynes, and terpenes. The alkane group of hydrocarbons constitutes the largest peak area represented in Table 5. Undecane,2-methyl-; Pentadecane; limonene and octadecane,2-methyl- demonstrated the highest peak percentages above 5% of 42.62, 6.74, 6.55, and 6.03, respectively. Limonene is a major terpene in the essential oil of *S. lancea*, as observed in Table 3.

The results represented above differed slightly from other studies due to various factors. Extraction method, temperature and storage conditions, soil characteristics, environmental factors, specific plant part used, ecosystem, time of harvest, and presence of contaminants are such factors responsible for a varying chemical composition. Compounds such as limonene are found to be present in all three plant extracts, which supports findings from other studies (Belhoussaine et al., 2022; Gundidza et al., 2009; Tyagi and Malik, 2011). The GC-MS analysis was only conducted on hexane extracts; however, volatile compounds may be found through other extraction solvents. These compounds include eucalyptol, which is the main component of *E. globulus*, mainly extracted through polar solvents. Hexane, due to its low polarity, allows the volatile compounds to spend less time interacting with the stationary phase of the GC column, ultimately leading to an improved separation of volatile compounds. Polar solvents nevertheless remain viable when handling compounds with a greater molecular weight.

3.4. In vitro antiviral activity studies

3.4.1. Neuraminidase activity assay

The neuraminidase activity test kit uses Amplex™ Red to detect hydrogen peroxide, produced by the oxidation of desialylated galactose by galactose oxidase. The final product of neuraminidase activity is the oxidation of galactose, and the enzyme plays a crucial role in releasing newly formed virions from the host cell membrane into the surrounding environment, leading to metastasis. Due to its role, it has become a key target in antiviral studies of influenza viruses (Do et al., 2023). Hexane, acetone, and methanol extracts were evaluated for antiviral activity, with hexane extracts showing the highest inhibition of neuraminidase activity. The subsequent quantified hexane extracts of *S. lancea* and *E. globulus* exhibited notable neuraminidase inhibition with IC_{50} values of 506 ± 21.00 and 526 ± 3.00 µg/mL, respectively, when compared to *S. molle*, which demonstrated the poorest activity with an IC_{50} value of 1326.00 ± 42.00 (Table 6). Compared to the positive control, the plant samples demonstrated poor activity with Oseltamivir having an IC_{50} of 3.529 ± 0.01 µg/mL.

The extracts of hexane, acetone, and methanol were evaluated for their inhibition of neuraminidase activity; however, only the hexane extracts expressed the best activity amongst the three. Due to the activity demonstrated by hexane extracts, it was then the preferred solvent of choice when conducting antiviral studies. The *S. lancea* extract exhibited the most notable anti-neuraminidase activity, expressed by an

Table 5
Chemical composition of the hexane extract of *Searsia lancea* leaves.

Functional group	Name	Retention times	Molecular weight	Molecular formula	Peak area %
Alcohols	Cyclohexanol, 2-methyl-5-(1-methylethenyl)-	4.16	154	$C_{10}H_{18}O$	1.35
	2,4-Decadien-1-ol	4.165	154	$C_{10}H_{18}O$	1.38
	1-Hexacosanol	5.145	382	$C_{26}H_{54}O$	1.29
	2-Decen-1-ol	4.41	156	$C_{10}H_{20}O$	1.25
	trans-2-Undecen-1-ol	4.885	170	$C_{11}H_{22}O$	1.30
	Phytol	15.57	296	$C_{20}H_{40}O$	0.94
Aldehydes	cis-4-Decenal	5.045	154	$C_{10}H_{18}O$	1.30
	6-Octenal, 3,7-dimethyl-	4.17	154	$C_{10}H_{18}O$	1.40
	2-Tridecenal, (E)-	5.04	196	$C_{13}H_{24}O$	1.13
	9-Octadecenal	5.455	266	$C_{18}H_{34}O$	1.19
	9,12,15-Octadecatrienal	15.99	262	$C_{18}H_{30}O$	0.76
Alkanes	Nonane	3.02	128	C_9H_{20}	2.44
	Pentadecane	4.705	212	$C_{15}H_{32}$	6.74
	Undecane, 2-methyl-	4.71	170	$C_{12}H_{26}$	42.62
	Octadecane, 2-methyl-	23.28	268	$C_{19}H_{40}$	6.03
	Hexatriacontane	18.53	506	$C_{36}H_{74}$	1.32
	Naphthalene, decahydro-2-methyl-	4.9	152	$C_{11}H_{20}$	1.09
Alkenes	1-Pentadecene, 2-methyl-	4.34	224	$C_{16}H_{32}$	1.30
	1-Decene, 4-methyl-	5.63	154	$C_{11}H_{22}$	2.80
	2-Methyl-n-1-tridecene	4.63	196	$C_{12}H_{28}$	1.29
	1-Nonene, 4,6,8-trimethyl-	4.39	168	$C_{12}H_{24}$	2.23
Alkynes	1-Dodecyne	4.89	166	$C_{12}H_{22}$	1.15
	1-Undecyne	4.895	152	$C_{11}H_{20}$	1.27
Cycloalkanes	Cyclohexane, 1,2,3-trimethyl-	4.65	126	C_9H_{18}	1.16
Cycloalkenes	1,12-Tridecadiene	5.03	180	$C_{13}H_{24}$	1.16
Epoxide	Oxirane, dodecyl-	4.8	212	$C_{14}H_{28}O$	1.13
Esters	2-Furancarboxylic acid, 4-pentadecyl ester	4.31	322	$C_{20}H_{34}O_3$	1.23
	Oxalic acid, allyl hexadecyl ester	4.755	354	$C_{21}H_{38}O_4$	1.34
Ether	Isooctane, (ethenyloxy)-	5.545	156	$C_{10}H_{20}O$	1.76
Halogenated alkane	2-Bromononane	4.45	206	$C_9H_{19}Br$	1.35
Ketone	2-Butanone, 4-cyclohexyl-	15.41	154	$C_{10}H_{18}O$	0.73
Terpene	Limonene	4.145	136	$C_{10}H_{16}$	6.55

Table 6
IC_{50} activity of the hexane extracts of selected medicinal plants against neuraminidase.

Medicinal plant	IC_{50} (µg/ml)
Eucalyptus globulus	526.00 ± 3.00
Schinus molle	1326.00 ± 42.00
Searsia lancea	506.00 ± 21.00
Oseltamivir	**3.529 ± 0.01****

Results are presented as mean values ± standard deviation; **Means significant difference with a $p < 0.0001$.

IC_{50} of 506 ± 21.00 µg/mL, followed by E. globulus (526 ± 3.00 µg/mL) and lastly S. molle (1326 ± 42.00 µg/mL), which had the poorest inhibition potential of neuraminidase activity. Statistically, the half-inhibitory concentration of *E. globulus* and *S. lancea* is similar. Research has shown that certain aromatic plants used in traditional medicine have potential anti-influenza properties and are commonly used to treat flu and related symptoms such as colds, coughs, sore throats, and bronchitis (Wu et al., 2012). However, the mechanisms of action of these aromatic plants are seldom reported. For example, 1,8-cineole (eucalyptol) found in *E. globulus*

has been reported to directly block neuraminidase activity (Mieres-Castro et al., 2021). The compound decreased the levels of inflammatory response markers intercellular adhesion molecule (ICAM)-1 and vascular cell adhesion molecule (VCAM)-1 in lung tissues (Ait-Ouazzou et al., 2011). Active compounds from selected medicinal plants attach to the active site of neuraminidase, hindering its interaction with sialic acid residues and therefore limiting its function. Furthermore, other phytochemical compounds bind to allosteric sites on the neuraminidase enzyme, altering its structure and preventing catalytic function, thereby decreasing its capacity to cleave sialic acid residues. *Eucalyptus globulus* also possesses antiviral activity emanating from its ability to modulate the immune system (Oriola and Oyedeji, 2022). This activity can enhance the host's immune defenses, leading to better viral clearance and reduced viral symptom severity (Oriola and Oyedeji, 2022).

The presence of phytochemical compounds has been shown to modulate cytokine production and release, signaling molecules that regulate immune responses (Ti, 2021). By influencing cytokine expression, these compounds can help regulate the balance between pro-inflammatory and anti-inflammatory immune responses (Ti, 2021). Some components of *Eucalyptus* essential oil may suppress cytokines that cause inflammation, such as tumor necrosis factor-alpha (TNF-alpha) and interleukin-6 (IL-6), while increasing the secretion of anti-inflammatory cytokines such as interleukin-10 (IL-10) (Arooj et al., 2023). A more balanced immune response can help mitigate excessive inflammation and tissue damage associated with viral infections (Arooj et al., 2023). Additionally, compounds from *E. globulus* have been reported to stimulate the activity of various immune cells, including macrophages, natural killer (NK) cells, and T lymphocytes (Shao et al., 2020). Macrophages play a crucial role in the innate immune response by engulfing and destroying pathogens, while NK cells and T lymphocytes are involved in the adaptive immune response by targeting virus-infected cells for destruction (Shao et al., 2020). By enhancing the function of these immune cells, Eucalyptus-derived compounds can strengthen the host's ability to produce an effective immune response against viral infections (Sandner et al., 2020). Studies have also shown that some compounds from *E. globulus* can induce the expression of interferons, thereby activating the antiviral state in surrounding cells and enhancing their resistance to viral infection (Mieres-Castro et al., 2021). Stimulation of the host's innate immune response to viral infections via this mechanism can enhance the overall antiviral activity of *Eucalyptus* extracts. Viral infections can occasionally trigger excessive or uncontrolled immune responses, leading to immunopathology and tissue damage. Immunomodulatory compounds from *E. globulus* help mitigate these adverse effects by regulating the intensity and duration of the immune response (Sandner et al., 2020).

3.4.2. Papain-like protease activity assay

The Papain-like protease assay kit is specifically intended to quantitatively evaluate the activity of Papain-like Protease. The quantified hexane extracts of *E. globulus*, *S. molle*, and *S. lancea* exhibited significant PL^{pro} inhibition activity with IC_{50} values of 70.175 ± 17.66, 60.5 ± 4.37, and 132.525 ± 1.41 µg/mL, respectively (Table 7). The results of the IC_{50} as observed in Table 7 suggests that *S. molle* portrayed notable activity in comparison to the other plant extracts. However, both *E. globulus* and *S. molle* achieved IC_{50} values below 100 µg/mL suggesting their strong potency against PL^{pro} (Chassagne et al., 2021).

Schinus molle is observed to be the most notable inhibitor of PL^{pro}, thereby limiting the activity of PL^{pro}. Among the three medicinal plant extracts, only *S. molle* and *E. globulus* demonstrated potent activity as observed from the IC_{50} value of potentially mimicking an inhibitor 5-amino-2-methyl-N-[(1R)-1-(1-naphthalenyl)ethyl]benzamide (GRL0617). The two plant samples have the potential of blocking the substrate from binding with the PL^{pro} enzyme, similar to GRL0617, which had an IC_{50} of 0.4870 µg/mL, which is significantly different from the medicinal plant extracts with a $p<0.0001$. The present phytochemicals, such as flavonoids and phenols, which possess antiviral properties, are attributed to the observed ability of these plant extracts to inhibit PLpro and disrupt its viral life cycle. Immunomodulatory compounds can boost the immune system's capacity to combat viral infections. While certain plant compounds possess virucidal properties, enabling them to directly deactivate viruses by reacting with the PL^{pro} enzyme. This enzyme plays a crucial role in cleaving large polyproteins at specific locations in the early stages of SARS-CoV-2 infection (Ghosh et al., 2023), thus leading to the production of vital nonstructural proteins necessary for virus replication (Ribaudo et al., 2023).

Table 7

IC_{50} activity of hexane extracts of the selected medicinal plants against PL^{pro}.

Medicinal plant	IC_{50} (µg/ml)
Eucalyptus globulus	70.175 ± 17.66
Schinus molle	60.5 ± 4.37
Searsia lancea	132.525 ± 1.41
5-Amino-2-methyl-N-[(1R)-1-(1-naphthalenyl)ethyl] benzamide (GRL0617)*	**0.4870****

Results are presented in mean values ± standard deviation; **Means significant difference with a $p < 0.0001$; *Data for GRL0617 is not specific as reported by manufacturer.

In addition to its main activity, PL^{pro} also serves as a deubiquitinating enzyme, allowing it to remove ubiquitin moieties from proteins (Cao et al., 2023). This distinctive function enables PLpro to modulate the host cell's immune response, potentially disrupting antiviral mechanisms. Eucalyptus leaves contain volatile oils, primarily composed of monoterpenoids such 1,8-cineole and α-pinene, as well as smaller amounts of sesquiterpenes, like globulol (Mieres-Castro et al., 2021). Steam inhalation of *Eucalyptus globulus* oil has been found to have a beneficial effect on alleviating symptoms associated with specific respiratory virus illnesses (Mieres-Castro et al., 2021).

3.5. Molecular modeling-mediated identification of bioactive constituents

The ligand selection for the in silico analysis followed the trend from *in vitro* analysis, where the hexane extracts of *E. globulus* and *S. lancea* were relatively more active against H1N1 neuraminidase, while *E. globulus* and *S. molle* were potent against PL^{pro}. The two-phase analysis included initial extra precision docking of the hexane constituents of these extracts as identified by GC-MS (Tables 3–5) followed by the extensive molecular dynamics simulation of potential hit(s). The highest binding energies of the compounds against both neuraminidase and SARS-CoV-2 receptors are represented in Table 8.

3.5.1. In silico identification of SARS-CoV-2 protease inhibitors

Docking against the first SARS-Cov-2 protease (7CMD) suggested 2,6,10,14-hexadecatetraen-1-ol, 3,7,11, 15-tetramethyl-, acetate, also known as geranylgeranyl acetate, as a potential 7CMD inhibitor with however a lower binding score (–3.363 kcal/mol) to that of the positive control (–6.551 kcal/mol). Geranylgeranyl acetate is a constituent of *S. molle* hexane extract (Table 4). The second predicted 7CMD inhibitor was ledol, a constituent of *E. globulus* hexane extract, with a binding score of –3.338 kcal/mol. Through its carboxyl oxygen, geranylgeranyl acetate formed two hydrogen bonds with Arg166 while Tyr268 contributed an aromatic hydrogen bond to the compound's binding pose (Figure 4A). Ledol could form only this Tyr268-mediated aromatic hydrogen bond (Figure 4B). On the other hand, positive control GRL0617 formed two hydrogen bonds involving Asp164 and GLN269. The binding conformation of GRL0617 was stabilized by the aromatic pi–pi bonds involving its three aromatic rings and Tyr268 (Figure 4C).

In the docking against a second SARS-CoV-2 protease, 7MB1, geranylgeranyl acetate was still identified as a potent SARS-CoV-2 protease inhibitor with similar binding score (–6.297 kcal/mol) to that of the positive control, GRL0617 (–6.504 kcal/mol). Geranylgeranyl acetate interacted with 7MB1 through a hydrogen bond from Hie163 residue (Figure 5A). The predicted second most active constituent was 1-tetracosanol from both *E. globulus* and *S. molle* hexane extracts (docking score: -6.224 kcal/mol) with two hydrogen bonds from Gln192 and Thr190 (Figure 5B). Similarly, GRL0617 attained a hydrogen bond from Thr190, and utilized its aromaticity to form aromatic hydrogen bond with Asp187 and a pi-pi bond with a catalytic site His41 (Figure 5C).

In general, docking against 7MB1 produced better docking scores for the test compounds while the positive control's binding score stayed relative the same between the two SARS-Cov-2 proteases. It was also notable that geranylgeranyl acetate maintained superior binding scores against both SARS-Cov-2 protease targets. Additionally, the binding scores of geranylgeranyl acetate and 1-tetracosanol against 7MB1

Table 8
Binding energies of selected compounds with the highest scores against neuraminidase (7MB1) and SARS-CoV-2 protease (1BJI) receptors.

Docking score (kcal/mol)			
Compound	**SARS-CoV-2 protease (7CMD)**	**SARS-CoV-2 protease (7MB1)**	**Neuraminidase (1BJI)**
2,6,10,14-Hexadecatetraen-1-ol, 3,7,11,15-tetramethyl-, acetate, (E,E,E)-	–3.363	–6.297	–2.414
Ledol	–3.338		–2.966
n-Tetracosanol		–-6.224	
Isopulegol			–2.531
2,4-Decadien-1-ol			–2.270
5-Amino-2-methyl-N-[(1R)-1-(1-naphthalenyl)ethyl]benzamide (GRL0617)	–6.551	–6.504	
Oseltamivir			–7.027

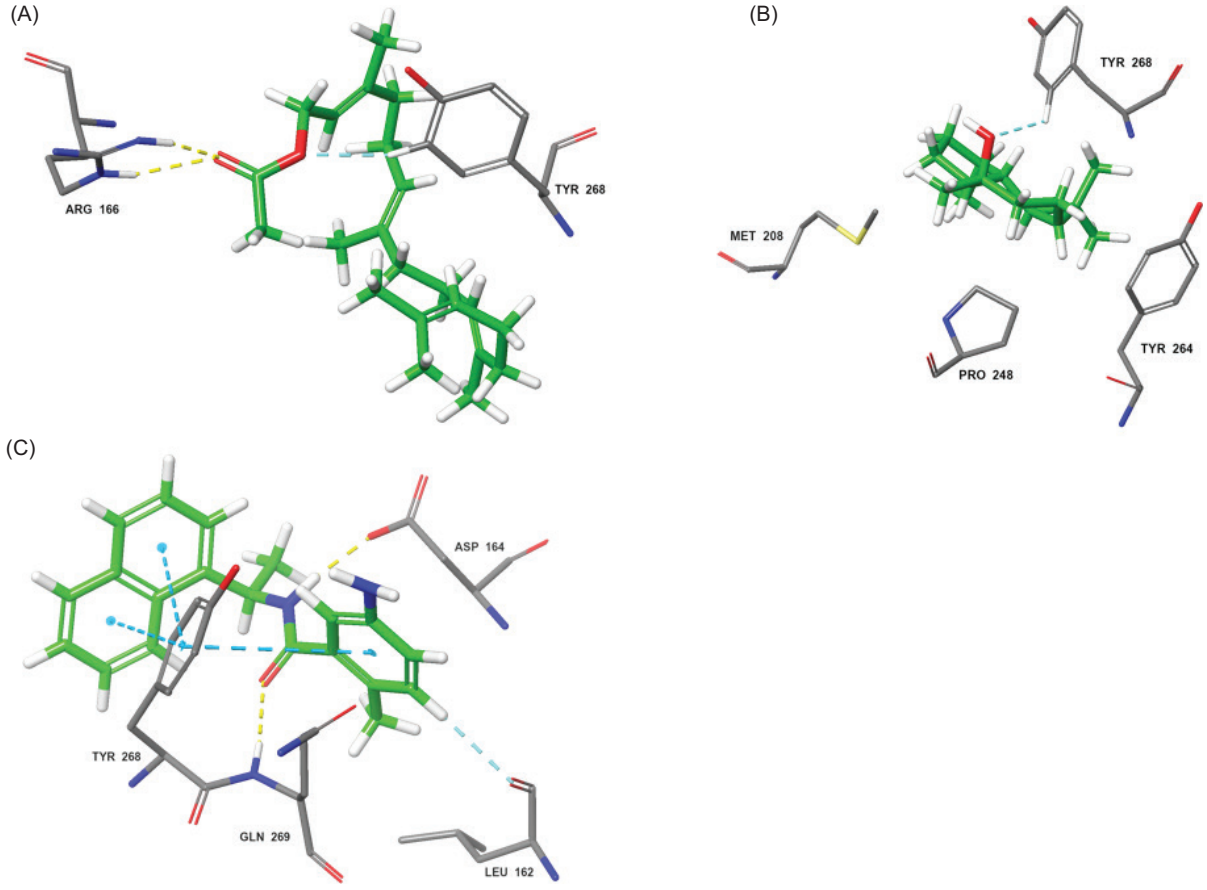

Figure 4. Extra precision docking results of geranylgeranyl acetate (A), ledol (B), and GRL0617 (positive control) (C) against SARS-Cov-2 7CMD.

were almost the same (–6.297 and –6.224 kcal/mol, respectively), and it was observed that their chemical structures have notable similarities including a long alkyl chain and one polar end; this may introduce a new class of SARS-Cov-2 protease inhibitors. For this reason, geranylgeranyl acetate and 1-tetracosanol were selected for 7MB1 binding accuracy and stability testing in the MM-GBSA and molecular dynamics platforms, respectively.

In the MM-GBSA redocking study, both geranylgeranyl acetate and 1-tetracosanol retained their binding conformations observed in the initial extra precision docking against 7MB1. Thus, geranylgeranyl acetate showed hydrogen bonding with Hie163 at a dG Bind score of –56.61 kcal/mol. Interestingly, 1-tetracosanol obtained a dG Bind score of –61.49 kcal/mol suggesting a higher binding affinity, evident from the strong hydrogen bonding coordination by Thr190-Gln192 (Figure 6). This confirms the higher accuracy of MM-GBSA-based dG Bind scoring algorithm in comparison to the empirical docking scores.

Apart from the binding stability assessment, the molecular dynamics calculations were also important to clarify if geranylgeranyl acetate and 1-tetracosanol established other interactions with 7MB1 including the expected nonpolar interactions with their alkyl chains. Nonpolar interactions often play a critical role in ligand trafficking to the active site (Rants'o et al., 2023). In the molecular dynamics assessment, the target receptor 7MB1 remained stable when in complex with either geranylgeranyl acetate or 1-tetracosanol as shown by protein root mean square deviations (RMSDs) that equilibrated below 3.0 Å (Figure 7A and 7B) (Al Khzem et al., 2025; Alturki et al., 2025). Though 7MB1 experienced some fluctuations between 90 and 100 ns when complexed with 1-tetraconasol, these were minor (RMSD ≤ 3.0) and short-lived (Figure 7B). Similarly, the RMSDs for both ligands remained steady throughout the 100 ns run signaling that the complexes were stable (Figure 7A and 7B).

In the dynamic mode, the frequent interactions between 7MB1 and geranylgeranyl acetate included hydrogen bonds involving Cys22 and Gly23, several water bridge-assisted hydrogen bonds involving Thr24-Thr26, His41, Ser46, Gly143, Ser144, Cys145, His163, Glu166, and Gln189, and hydrophobic bonds from Leu27, Cys44, Met49,

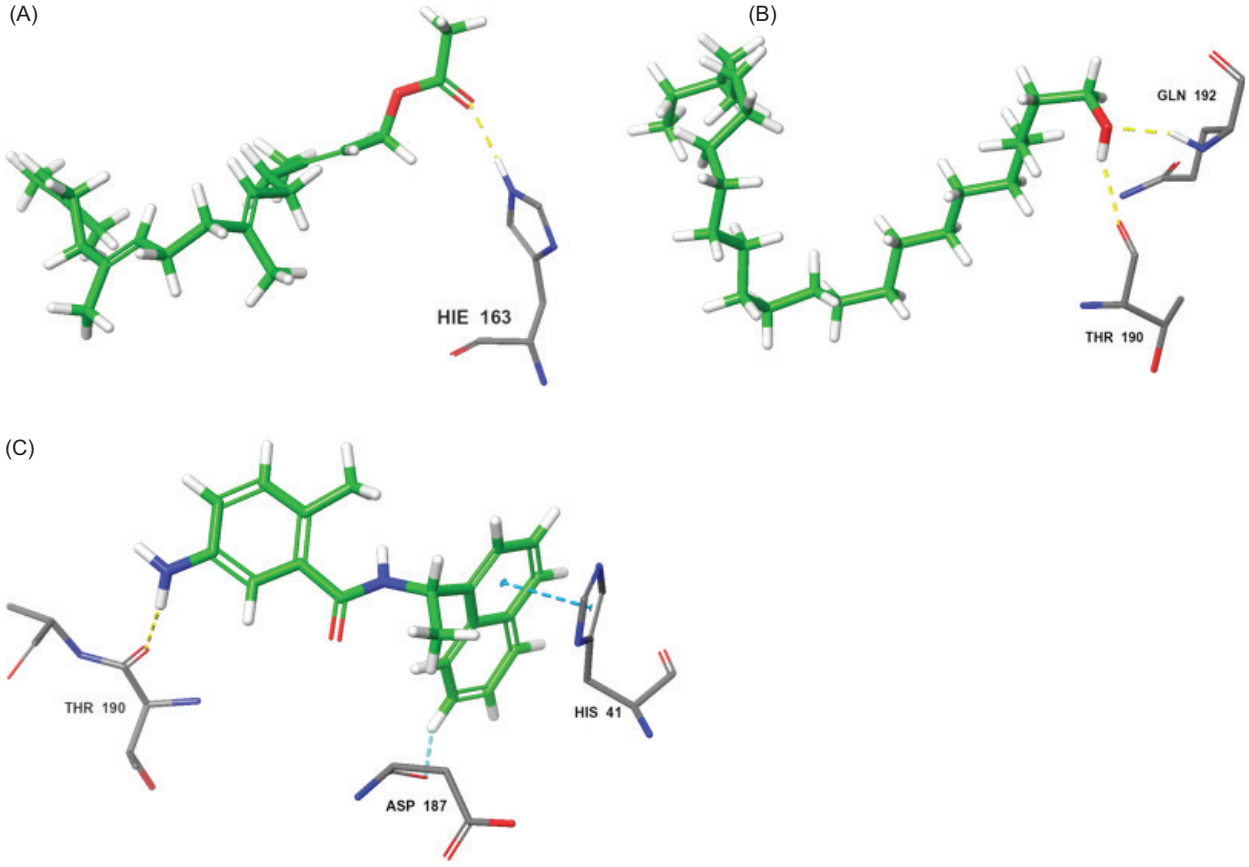

Figure 5. Extra precision docking results of geranylgeranyl acetate (A), 1-tetracosanol (B), and GRL0617 (C) against SARS-Cov-2 7MB1.

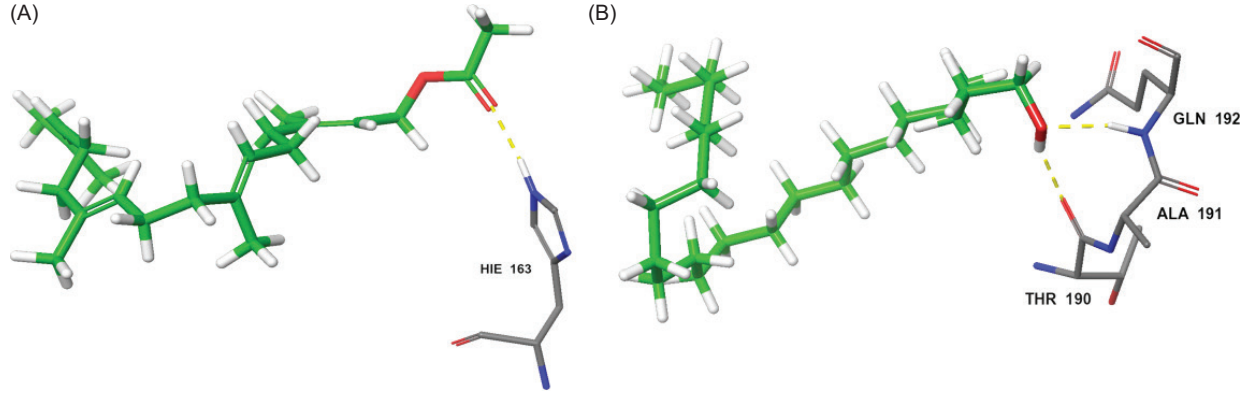

Figure 6. MM-GBSA redocking results of geranylgeranyl acetate (A) and 1-tetracosanol (B) against the 7MB1 SARS-Cov-2 protease.

Cys145, Met165, and Pro168 (Figure 8A and 8B). Similarly, 1-tetracosanol constantly established water bridge-supplemented hydrogen bonds involving Thr24-Thr26, His41, Ser46, Asn119, Asn142, Gly143, Glu166, Arg188, Gln189, Thr190, and Gln192 (Figure 8C and 8D).

The 1-tetracosanol-7MBD complex was also maintained by frequent hydrophobic bonds involving Cys44, Met49, Met165, Leu167, and Pro168. In general, the 7MB1 binding conformation of geranylgeranyl acetate and 1-tetracosanol had their long alkyl chains involved in hydrophobic interactions with the protein's hydrophobic amino acid residues, mainly Met49 and Met165, and their polar ends involved in hydrogen bonds; the carboxylic acid ester of geranylgeranyl acetate mainly interacted with Cys22, Gly23, Thr26, and

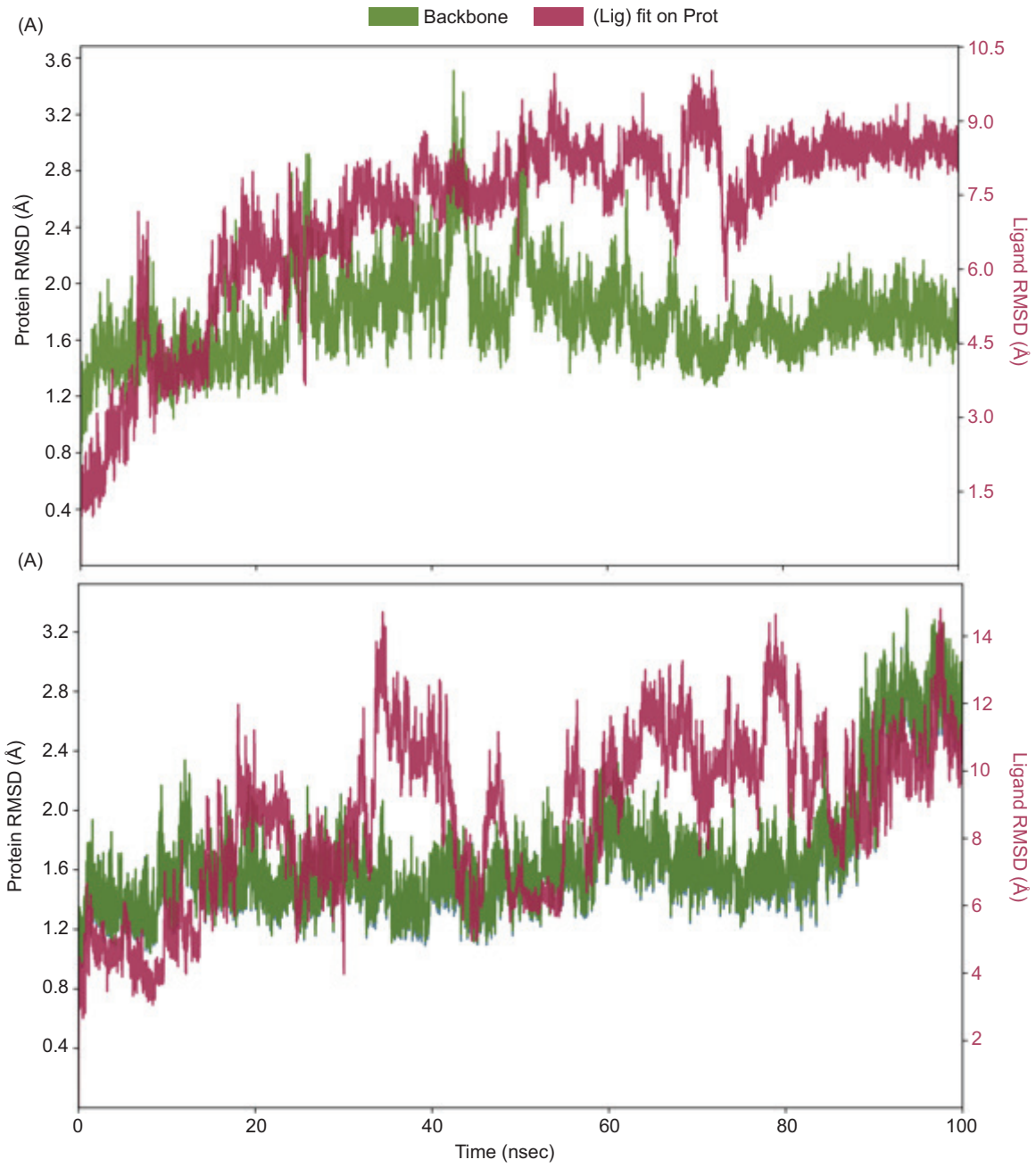

Figure 7. Binding stability testing displayed by fluctuations of the 7MB1 backbone and ligands geranylgeranyl acetate (A) and 1-tetracosanol (B) during the molecular dynamics simulation.

Glu166 while the hydroxyl group of 1-tetracosanol maintained its interaction with Gln192 and Thr25.

While the hydrophobic portions of geranylgeranyl acetate and 1-tetracosanol seemed to interact with the same amino acid residues, there was a clear distinction on the amino acid residues interacting with the polar groups of the compounds; this indicated that their binding conformations may be slightly different. This is possible because the active site of SARS-Cov-2 protease 7MB1 has several sub-pockets known as subsites, two of which express the catalytic residues His41 and Cys145 (Lockbaum et al., 2021). Indeed, while the alkyl portions of geranylgeranyl acetate (orange) and 1-tetracosanol (green) were configured between Met49 and Met165, the polar end of geranylgeranyl acetate occupied the subsite marked by Glu166 and 1-tetracosanol preferred the Pro168 subsite (Figure 9).

The Pro168 subsite was also a preferred site for the polar amine group of the positive control GRL0617 (red). In

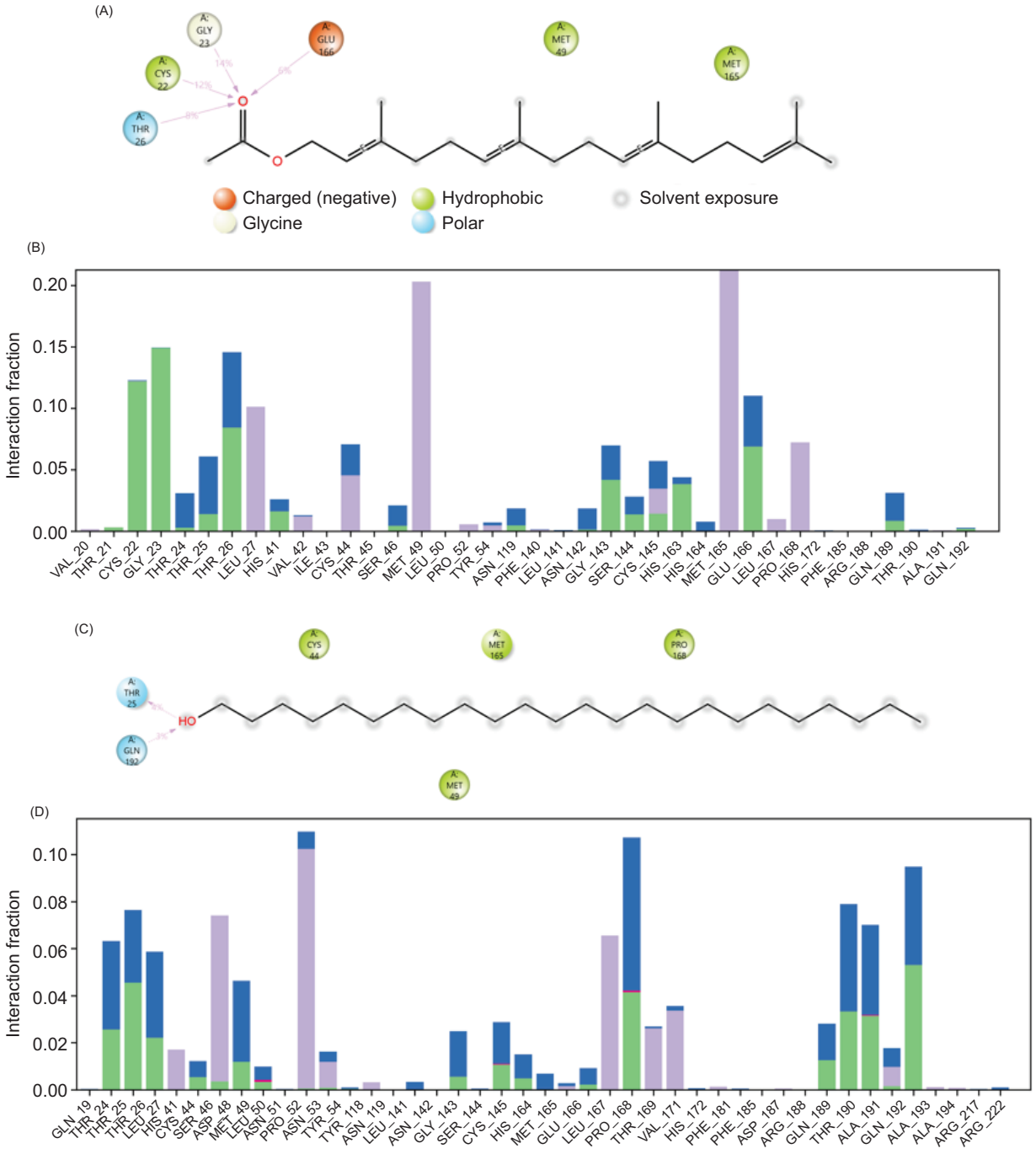

Figure 8. Frequent molecular interactions of the SARS-Cov-2 target (7MB1) with geranylgeranyl acetate (A and B) and 1-tetracosanol (C and D).

agreement with the extra precision docking results (Figure 5), the fused ring portion of GRL0617 interacted with the catalytic His41 subsite. Remarkably, geranylgeranyl acetate and 1-tetracosanol interacted with the catalytic subsites where the former favored the His41 subsite, and the latter occupied the Cys145 subsite (Figure 9). This may explain their potent activity of the hexane extracts containing these constituents against SARS-Cov-2 protease *in vitro*.

3.5.2. In silico *identification of H1N1 neuraminidase inhibitors*

Both the *E. globulus* and *S. lancea* hexane extracts inhibited H1N1 neuraminidase at IC_{50} value of approximately 500

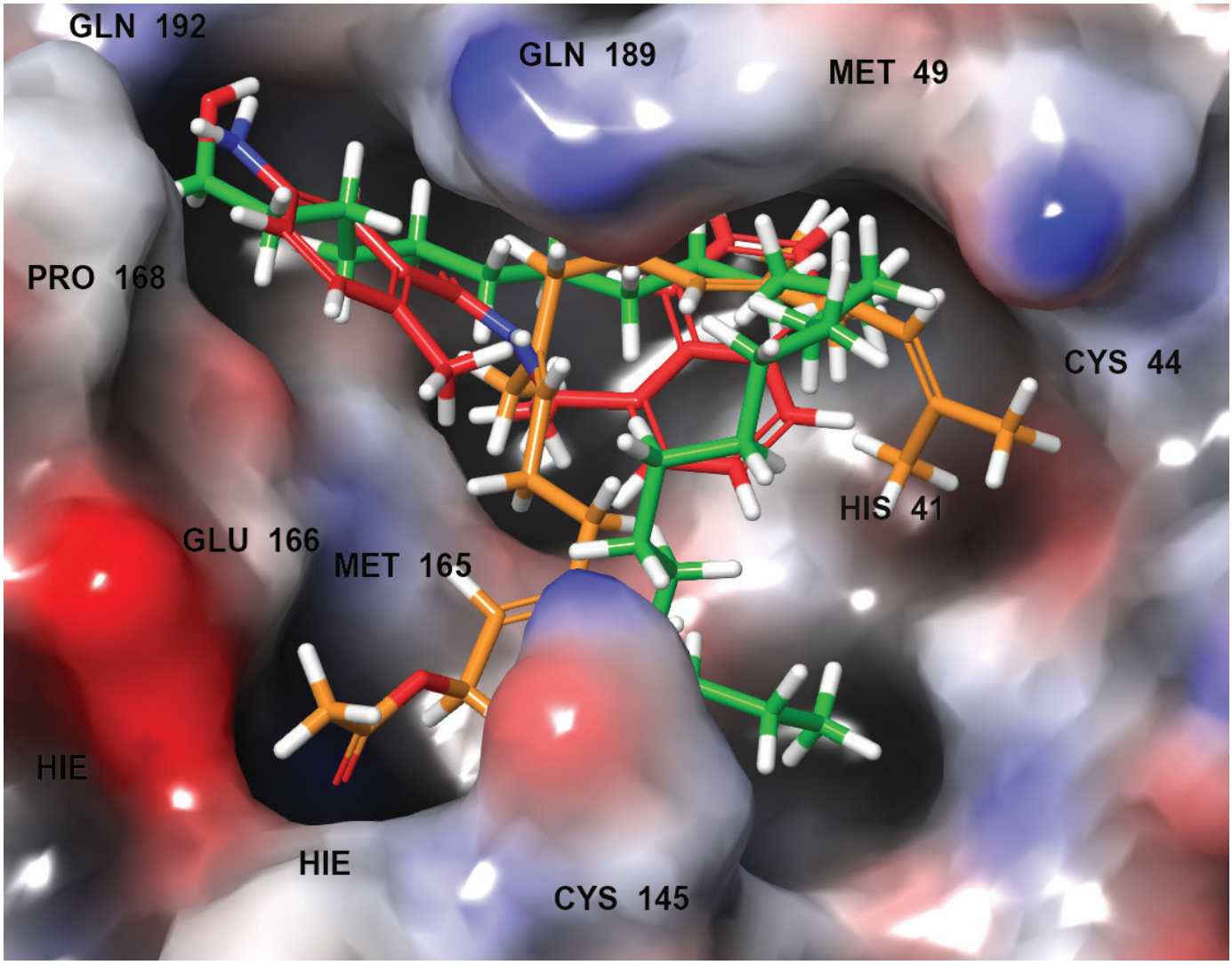

Figure 9. Comparison of the 7MB1 binding poses of geranylgeranyl acetate (orange) 1-tetracosanol (green), and GRL0617 (red).

µg/mL (Table 7). Ledol obtained the highest binding score of –2.966 kcal/mol, however, this was an exclusive constituent of *E. globulus* hexane extract (Table 3). We looked for a common constituent in both *E. globulus* and *S. lancea* that may be responsible for the observed activity. Accordingly, at least two constituents of both *E. globulus* and *S. lancea* that obtained the highest binding scores against the neuraminidase target were isopulegol (–2.531 kcal/mol) and 2,4-decadien-1-ol (–2.270 kcal/mol). However, these scores were much lower than that of the positive control, oseltamivir (–7.027 kcal/mol), suggesting that these constituents may have lower binding affinity towards 1BJI. Like ledol, isopulegol could only form a water-assisted hydrogen bond through their hydroxyl groups while 2,4-decadien-1-ol established at least two hydrogen bounds with Tyr406 and Arg361 residues (Figure 10A–10C). Conversely, oseltamivir was superior with six hydrogen bonds and two electrostatic interactions contributing to its favorable binding (Figure 10D).

Even though terpenoids are notorious with low binding scores in docking applications even when their potency has been confirmed by the biological assays (Rants'o et al., 2023), our *in silico* data agreed with the *in vitro* results, where both *E. globulus* and *S. lancea* obtained inactive IC_{50} values > 100 µg/mL (Chassagne et al., 2021) while oseltamivir attained a lower IC_{50} of 3.529 ± 0.01 µg/mL (Table 7). For this reason, the molecular dynamics-based binding stability of any of these constituents against IBJI was not pursued.

3.5.3. Molecular modeling-mediated prediction of bioactive constituents

The *in vitro* screening data indicated that the hexane extracts of *E. globulus* and *S. molle* were potent against

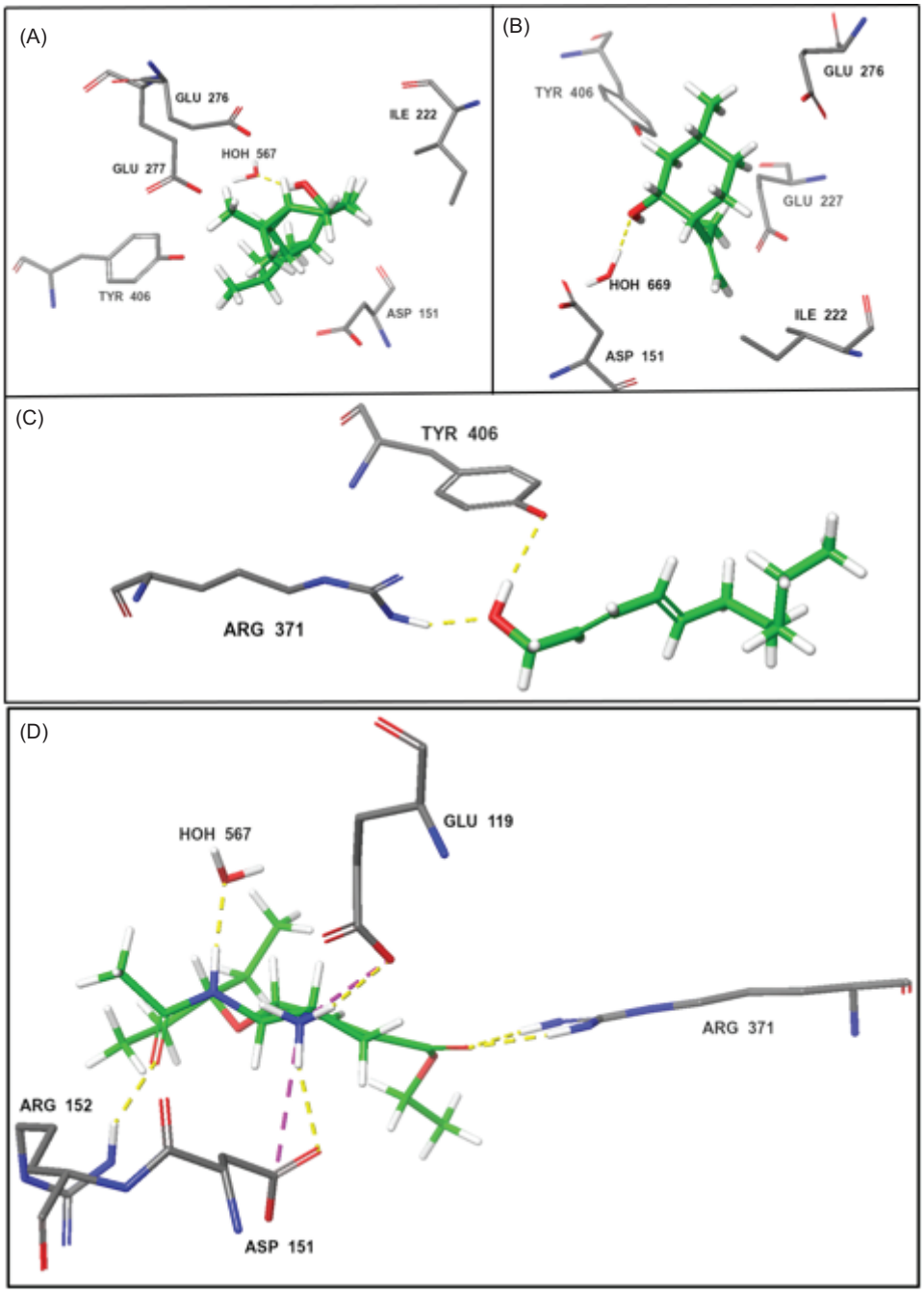

Figure 10. Extra precision docking results of ledol (A), isopulegol (B), 2,4-decadien-1-ol (C), and oseltamivir (positive control) (D) against H1N1 1BJI.

SARS-Cov-2 protease (Table 8). Thus, the *in silico* docking screened the constituents of these extracts as identified by GC-MS (Tables 3 and 4) against two principal SARS-Cov-2 proteases (PDB: 7CMD and 7MB1) that complementarily hydrolyse the viral polyproteins during replication (Narayanan et al., 2022). In the initial extra precision screening, the *E. globulus* constituent geranylgeranyl acetate emerged as a potential inhibitor of both proteases, with its affinity leaning towards 7MB1, where its binding score matched that of the positive control, GRL0617. Interestingly, another constituent from both *E. globulus* and *S. molle* hexane extracts, 1-tetracosanol, had a similar affinity to geranylgeranyl acetate and GRL0617. Nevertheless, the MM-GBSA-mediated redocking studies showed that more hydrogen bonds established by 1-tetracosanol against 7MB1 granted it a higher binding affinity than geranylgeranyl acetate.

Binding stability assessment through molecular dynamics showed that the 7MB1 complexes with geranylgeranyl acetate and 1-tetracosanol remained stable throughout the 100 ns simulation (Figure 7). Furthermore, the molecular dynamics analysis displayed that geranylgeranyl acetate strikingly interacted with the recognized key amino acid residues in the SARS-Cov-2 protease active site, such as Gly143, Ser144, Cys145, His163, and Glu166 (Aminah et al., 2021; Venugopal and Chakraborty, 2022; Yan et al., 2024). Further docking visualizations (Figure 9) identified that this is caused by its preferred configuration that places its carboxylic acid ester in the Glu166-based active site sub-pocket. Conversely, 1-tetracosanol's hydroxyl group occupied the subsite marked by Pro168, where it predominantly interacted with Arg188, Gln189, Thr190, and Gln192. Another notable advantage of the long alkyl chains of geranylgeranyl acetate and 1-tetracosanol was their ability to interact with the catalytic subsites marked by His41 and Cys145 (Figure 9).

Conversely, the *E. globulus* and *S. lancea* hexane extracts were relatively active against H1N1 neuraminidase (Table 7). However, the activity of *E. globulus* and *S. lancea* hexane extracts against H1N1 neuraminidase was low, with IC_{50} values ~500 µg/mL. In agreement with this, the in silico docking of the GC-MS-identified constituents (Tables 3 and 5) of *E. globulus* and *S. lancea* hexane extracts could not identify any constituent with a docking score closer to, or above, that of the positive control, oseltamivir. Similarly, none of the three compounds with the relatively highest scores against neuraminidase 1BJI assumed the binding conformation similar to that of oseltamivir (Figure 10).

4. CONCLUSIONS

Total phenolic and flavonoid content showed the presence of both phenolic compounds and flavonoids in all three plant samples at varying quantities, with *E. globulus* and *S. lancea* demonstrating the highest possession in both classes. Eucalyptus globulus proved to be the best candidate to act as a ferric ion reducer, S. molle proved to be the best hydrogen peroxide scavenger, while *S. lancea* proved to be the best candidate to act as a DPPH radical scavenger, as observed from the %RSA recordings. GC-MS analysis determined the chemical composition of non-polar volatile compounds potentially found in the selected medicinal plants, with hydrocarbons constituting the highest % peak area. The non-polar compounds of *E. globulus, S. molle*, and *S. lancea* have been demonstrated to possess notable antineuraminidase and anti-PL^{pro} properties, with *E. globulus* acting as the best candidate among the three. In silico studies identified geranylgeranyl acetate from *S. molle* and 1-tetracosanol from both *E. globulus* and *S. molle* as potential inhibitors of SARS-Cov-2 protease (PDB: 7MB1), given their striking interaction with key active site residues and binding affinities closer to that of the positive control, GRL0617. These results suggest in vitro and in vivo validation of the anti-SARS-CoV-2 protease activities of geranylgeranyl acetate and 1-tetracosanol.

PATENT

A provisional patent application has been filed in South Africa with the reference number 2025/01633.

ACKNOWLEDGEMENTS

Authors would like to acknowledge Center for High Performance Computing (CHPC; Cape Town, South Africa) for offering us a platform to conduct extensive *in silico* analyses reported in this study.

FUNDING

This research was funded by National Research Foundation (South Africa), grant numbers TTK2203311482.

CONFLICT OF INTEREST STATEMENT

The authors declare no conflicts of interest.

INSTITUTIONAL REVIEW BOARD STATEMENT

The study was conducted in accordance with the Declaration of Helsinki, and approved by the Ethics Committee of Sefako Makgatho Health Sciences University (SMUREC/S/404/2022:PG).

ORCID

Lesiba Thabo Lekgoathi	0000-0001-8898-7230
Sechene Stanley Gololo	0000-0002-8059-1941
Thankhoe Abram Rants'o	0000-0001-8585-0888
Lefa Julius Lerotholi	0000-0003-1278-6963
Xavier Siwe-Noundou	0000-0002-8667-8351
Vuyisile Samuel Thibane	0000-0001-9169-9379

REFERENCES

Ait-Ouazzou, A., Lorán, S., Bakkali, M., Laglaoui, A., Rota, C., Herrera, A., Pagán, R., Conchello, P., 2011. Chemical composition and antimicrobial activity of essential oils of *Thymus algeriensis, Eucalyptus globulus* and *Rosmarinus officinalis* from Morocco. Journal of the Science of Food and Agriculture 91, 2643–2651. https://doi.org/10.1002/jsfa.4505

Al Khzem, A.H., Shoaib, T.H., Mukhtar, R.M., Alturki, M.S., Gomaa, M.S., Hussein, D., Tawfeeq, N., Bano, M., Sarafroz, M., Alzahrani, R., Alghamdi, H., Rants'o, T.A., 2025. Repurposing FDA-Approved Agents to Develop a Prototype Helicobacter pylori Shikimate Kinase (HPSK) Inhibitor: A Computational Approach Using Virtual Screening, MM-GBSA Calculations, MD Simulations, and DFT Analysis. Pharmaceuticals 18, 174. https://doi.org/10.3390/ph18020174

Almas, I., Innocent, E., Machumi, F., Kisinza, W., 2021. Chemical composition of essential oils from *Eucalyptus globulus* and *Eucalyptus maculata* grown in Tanzania. Scientific African 12, e00758. https://doi.org/10.1016/j.sciaf.2021.e00758

Alturki, M.S., Tawfeeq, N., Alissa, A., Ahbail, Z., S. Gomaa, M., Al Khzem, A.H., Rants'o, T.A., Akbar, M.J., Alharbi, W.S., Alshehri, B.Y., Alotaibi, A.N., Almughem, F.A., Alshehri, A.A., 2025. Targeting KRAS G12C and G12S Mutations in Lung Cancer: *In Silico* Drug Repurposing and Antiproliferative Assessment on A549 Cells. Informatics in Medicine Unlocked 52, 101612. https://doi.org/10.1016/j.imu.2024.101612

Aminah, N.S., Abdjan, M.I., Wardana, A.P., Kristanti, A.N., Siswanto, I., Rakhman, K.A., Takaya, Y., 2021. The dolabellane diterpenes as potential inhibitors of the SARS-CoV-2 main protease: molecular insight of the inhibitory mechanism through computational studies. RSC Advances 11, 39455–39466. https://doi.org/10.1039/D1RA07584E

Antony, P., Vijayan, R., 2021. Molecular dynamics simulation study of the interaction between human angiotensin converting enzyme 2 and spike protein receptor binding domain of the SARS-CoV-2 B.1.617 variant. Biomolecules 11, 1–10. https://doi.org/10.3390/biom11081244

Arooj, B., Asghar, S., Saleem, M., Khalid, S.H., Asif, M., Chohan, T., Khan, I.U., Zubair, H.M., Yaseen, H.S., 2023. Anti-inflammatory mechanisms of eucalyptol rich *Eucalyptus globulus* essential oil alone and in combination with flurbiprofen. Inflammopharmacology 31, 1849–1862. https://doi.org/10.1007/s10787-023-01237-6

Astani, A., Schnitzler, P., 2014. Antiviral activity of monoterpenes beta-pinene and limonene against herpes simplex virus *in vitro*. Iranian Journal of Microbiology 6, 149–55.

Awouafack, M.D., Tane, P., Morita, H., 2017. Isolation and structure characterization of flavonoids, in: Flavonoids - From Biosynthesis to Human Health. InTech. https://doi.org/10.5772/67881

Belhoussaine, O., El Kourchi, C., Harhar, H., Bouyahya, A., El Yadini, A., Fozia, F., Alotaibi, A., Ullah, R., Tabyaoui, M., 2022. Chemical composition, antioxidant, insecticidal activity, and comparative analysis of essential oils of leaves and fruits of *Schinus molle* and *Schinus terebinthifolius*. Evidence-Based Complementary and Alternative Medicine 2022, 1–12. https://doi.org/10.1155/2022/4288890

Bvenura, C., Kambizi, L., 2022. Composition of phenolic compounds in South African *Schinus molle* L. berries. Foods 11, 1376. https://doi.org/10.3390/foods11101376

Çalişkan, B., Çalişkan, A.C., 2021. Antioxidant and oxidative stress, in: Antioxidants - Benefits, Sources, Mechanisms of Action. IntechOpen. https://doi.org/10.5772/intechopen.96643

Cao, D., Duan, L., Huang, B., Xiong, Y., Zhang, G., Huang, H., 2023. The SARS-CoV-2 papain-like protease suppresses type I interferon responses by deubiquitinating STING. Sci Signal 16. https://doi.org/10.1126/scisignal.add0082

Caruso, A.A., Del Prete, A., Lazzarino, A.I., 2020. Hydrogen peroxide and viral infections: A literature review with research hypothesis definition in relation to the current COVID-19 pandemic. Medical Hypotheses 144, 109910. https://doi.org/10.1016/j.mehy.2020.109910

Chassagne, F., Samarakoon, T., Porras, G., Lyles, J.T., Dettweiler, M., Marquez, L., Salam, A.M., Shabih, S., Farrokhi, D.R., Quave, C.L., 2021. A Systematic Review of Plants With Antibacterial Activities: A Taxonomic and Phylogenetic Perspective. Frontiers in Pharmacology 11, 586548. https://doi.org/10.3389/fphar.2020.586548

Chaves, N., Santiago, A., Alías, J.C., 2020. Quantification of the antioxidant activity of plant extracts: Analysis of sensitivity and hierarchization based on the method used. Antioxidants 9, 76. https://doi.org/10.3390/antiox9010076

Chen, K.K., Minakuchi, M., Wuputra, K., Ku, C.-C., Pan, J.-B., Kuo, K.-K., Lin, Y.-C., Saito, S., Lin, C.-S., Yokoyama, K.K., 2020. Redox control in the pathophysiology of influenza virus infection. BMC Microbiology 20, 214. https://doi.org/10.1186/s12866-020-01890-9

Chia, B., Lim, S.P., 2023. A patent review on SARS Coronavirus papain-like protease (PL^{pro}) inhibitors. ChemMedChem 18, e202300216. https://doi.org/10.1002/cmdc.202300216

Corrêa, A.N.Ribeiro., Weimer, Patrícia., Rossi, R.Cassanta., Hoffmann, J.F., Koester, L.S., Suyenaga, E.S., Ferreira, C.D., 2023. Lime and orange essential oils and d-limonene as a potential COVID-19 inhibitor: Computational, in chemico, and cytotoxicity analysis. Food Bioscience 51, 102348. https://doi.org/10.1016/j.fbio.2022.102348

Dezsi, Ştefan, Bădărău, A., Bischin, C., Vodnar, D., Silaghi-Dumitrescu, R., Gheldiu, A.-M., Mocan, A., Vlase, L., 2015. Antimicrobial and antioxidant activities and phenolic profile of *Eucalyptus globulus* Labill. and *Corymbia ficifolia* (F. Muell.) K.D. Hill & amp; L.A.S. Johnson leaves. Molecules 20, 4720–4734. https://doi.org/10.3390/molecules20034720

Do, T.H.T., Wheatley, A.K., Kent, S.J., Koutsakos, M., 2023. Influenza B virus neuraminidase: A potential target for next-generation vaccines? Expert Reviews of Vaccines 23, 39–48. https://doi.org/10.1080/14760584.2023.2290691

Dong, W., Wei, X., Zhang, F., Hao, J., Huang, F., Zhang, C., Liang, W., 2014. A dual character of flavonoids in influenza A virus replication and spread through modulating cell-autonomous immunity by MAPK signaling pathways. Frontiers in Immunology 4, 7237. https://doi.org/10.1038/srep07237

Dumas, A., Knaus, U.G., 2021. Raising the 'good' oxidants for immune protection. Frontiers in Immunology 12, 698042. https://doi.org/10.3389/fimmu.2021.698042

Fadilah, N.Q., Jittmittraphap, A., Leaungwutiwong, P., Pripdeevech, P., Dhanushka, D., Mahidol, C., Ruchirawat, S., Kittakoop, P., 2022. Virucidal activity of essential oils from *Citrus x aurantium* L. against influenza A virus H1N1: limonene as a potential household disinfectant against virus. Natural Production Communications 17, 1934578X2110727. https://doi.org/10.1177/1934578X211072713

Fernandes, R.P.P., Trindade, M.A., Tonin, F.G., Lima, C.G., Pugine, S.M.P., Munekata, P.E.S., Lorenzo, J.M., de Melo, M.P., 2016. Evaluation of antioxidant capacity of 13 plant extracts by three different methods: Cluster analyses applied for selection of the natural extracts with higher antioxidant capacity to replace synthetic

antioxidant in lamb burgers. Journal of Food Science and Technology 53, 451–460. https://doi.org/10.1007/s13197-015-1994-x

Fernando, C.D., Soysa, P., 2015. Optimized enzymatic colorimetric assay for determination of hydrogen peroxide (H_2O_2) scavenging activity of plant extracts. MethodsX 2, 283–291. https://doi.org/10.1016/j.mex.2015.05.001

Frolova, N., Ukrainets, A., Sylka, I., Nemirich, A., Kuzmin, O., 2019. Separation of terpenes from lemon essential oil by selective fractionation under a vacuum. Eastern-European Journal of Enterprise Technologies 2, 32–36. https://doi.org/10.15587/1729-4061.2019.160220

Ghosh, A.K., Shahabi, D., Imhoff, M.E.C., Kovela, S., Sharma, A., Hattori, S., Higashi-Kuwata, N., Mitsuya, H., Mesecar, A.D., 2023. SARS-CoV-2 papain-like protease (PL^{pro}) inhibitory and antiviral activity of small molecule derivatives for drug leads. Bioorganic & Medicinal Chemistry Letters 96, 129489. https://doi.org/10.1016/j.bmcl.2023.129489

Girard, M.P., Tam, J.S., Assossou, O.M., Kieny, M.P., 2010. The 2009 a (H1N1) influenza virus pandemic: a review. Vaccine 28, 4895–4902. https://doi.org/10.1016/j.vaccine.2010.05.031

Gololo, S.S., Mapfumari, N.S., Sethoga, L., Olivier, M., Mogale, M.A., 2016. Identification of Phytochemical Constituents within the N-Hexane Leaf Extract of *Senna italica* (Mill) using Gas Chromatography-Mass Spectrometry (GC-MS) analysis. Journal of Pharmaceutical Sciences and Research 8, 1141–1143.

González-Palma, I., Escalona-Buendía, H.B., Ponce-Alquicira, E., Téllez-Téllez, M., Gupta, V.K., Díaz-Godínez, G., Soriano-Santos, J., 2016. Evaluation of the antioxidant activity of aqueous and methanol extracts of *Pleurotus ostreatus* in different growth stages. Frontiers in Microbiology 7, 1099–1108. https://doi.org/10.3389/fmicb.2016.01099

Gundidza, N., Gweru, N., Magwa, M.L., Mmebengwa, V., Samie, A., 2009. The chemical composition and biological activities of essential oil from the fresh leaves of *Schinus terebinthifolius* from Zimbabwe. African Journal of Biotechnology 8, 7164–7169.

Himed, L., Merniz, S., Monteagudo-Olivan, R., Barkat, M., Coronas, J., 2019. Antioxidant activity of the essential oil of *Citrus limon* before and after its encapsulation in amorphous SiO2. Scientific African 6, e00181. https://doi.org/10.1016/j.sciaf.2019.e00181

Hu, Q., Xiong, Y., Zhu, G., Zhang, Ya-Ni, Zhang, Yi-Wen, Huang, P., Ge, G., 2022. The SARS-CoV-2 main protease (M^{pro}): Structure, function, and emerging therapies for COVID-19. MedComm (Beijing) 3, e151. https://doi.org/10.1002/mco2.151

Hyland, R.A., Rogers, P.J., Higgins, V.J., Myers, S., Coorssen, J.R., 2012. Measuring hydrogen peroxide reduction using a robust, inexpensive, and sensitive method. Journal of Chemical Biology 5, 143–150. https://doi.org/10.1007/s12154-012-0083-0

Jacek, C., Karolina, S., Orzeł, A., Frączek, M., Tomasz, Z., 2021. Comparison of the clinical differences between COVID-19, SARS, influenza, and the common cold: A systematic literature review. Advances in Clinical and Experimental Medicine 30, 109–114. https://doi.org/10.17219/acem/129573

Jayaprakasha, G.K., Jaganmohan Rao, L., Sakariah, K.K., 2004. Antioxidant activities of flavidin in different *in vitro* model systems. Bioorganic & Medicinal Chemistry 12, 5141–5146. https://doi.org/10.1016/j.bmc.2004.07.028

Jerbi, A., Derbali, A., Elfeki, A., Kammoun, M., 2017. Essential oil composition and biological activities of *Eucalyptus globulus* leaves extracts from Tunisia. Journal of Essential Oil Bearing Plants 20, 438–448. https://doi.org/10.1080/0972060X.2017.1304832

Jha, N.K., Sharma, C., Hashiesh, H.M., Arunachalam, S., Meeran, M.N., Javed, H., Patil, C.R., Goyal, S.N., Ojha, S., 2021. β-Caryophyllene, a natural dietary CB2 receptor selective Cannabinoid can be a candidate to target the trinity of infection, immunity, and inflammation in COVID-19. Frontiers in Pharmacology 12, 590201. https://doi.org/10.3389/fphar.2021.590201

Jhaveri, R., 2020. Echoes of 2009 H1N1 influenza pandemic in the COVID pandemic. . Clinical Therapeutics 42, 736–740. https://doi.org/10.1016/j.clinthera.2020.04.003

Karioti, A., Hadjipavlou-Litina, D., Mensah, M.L.K., Fleischer, T.C., Skaltsa, H., 2004. Composition and antioxidant activity of the essential oils of *Xylopia aethiopica* (Dun) A. Rich. (Annonaceae) leaves, stem bark, root bark, and fresh and dried fruits, growing in Ghana. Journal of Agricultural and Food Chemistry 52, 8094–8098. https://doi.org/10.1021/jf040150j

Kim, D.H., Park, M.H., Choi, Y.J., Chung, K.W., Park, C.H., Jang, E.J., An, H.J., Yu, B.P., Chung, H.Y., 2013. Molecular study of dietary heptadecane for the anti-inflammatory modulation of NF-kB in the aged kidney. PLoS One 8, e59316. https://doi.org/10.1371/journal.pone.0059316

Koki, M., Yalo, M., Makhaba, M., Nako, N., Rautenbach, F., Badmus, J.A., Marnewick, J., Hussein, A.A., Mabusela, W.T., 2022. Phytochemical investigation and biological studies on selected *Searsia* species. Plants 11, 2793. https://doi.org/10.3390/plants11202793

Lim, T.Y., Lim, Y.Y., Yule, C.M., 2009. Evaluation of antioxidant, antibacterial and anti-tyrosinase activities of four *Macaranga* species. Food Chemistry 114, 594–599.

Lin, D., Xiao, M., Zhao, J., Li, Z., Xing, B., Li, X., Kong, M., Li, L., Zhang, Q., Liu, Y., Chen, H., Qin, W., Wu, H., Chen, S., 2016. An overview of plant phenolic compounds and their importance in human nutrition and management of type 2 diabetes. Molecules 21, 1374. https://doi.org/10.3390/molecules21101374

Lockbaum, G.J., Reyes, A.C., Lee, J.M., Tilvawala, R., Nalivaika, E.A., Ali, A., Kurt Yilmaz, N., Thompson, P.R., Schiffer, C.A., 2021. Crystal Structure of SARS-CoV-2 Main Protease in Complex with the Non-Covalent Inhibitor ML188. Viruses 13, 174. https://doi.org/10.3390/v13020174

Magwede, K., Van Wyk, B.-E., 2016. An inventory of Vhavenda useful plants, Limpopo Province, South Africa. South African Journal of Botany 103, 325. https://doi.org/10.1016/j.sajb.2016.02.083

Massova, I., Kollman, P.A., 2000. Combined molecular mechanical and continuum solvent approach (MM-PBSA/GBSA) to predict ligand binding. Perspectives in drug discovery and design 18, 113–135.

Mathew, S., Abraham, T.E., Zakaria, Z.A., 2015. Reactivity of phenolic compounds towards free radicals under *in vitro* conditions. Journal of Food Science and Technology 52, 5790–5798. https://doi.org/10.1007/s13197-014-1704-0

Mazik, M., 2022. Promising therapeutic approach for SARS-CoV-2 infections by using a rutin-based combination therapy. ChemMedChem 17, e202200157. https://doi.org/10.1002/cmdc.202200157

McClain, C.B., Vabret, N., 2020. SARS-CoV-2: The many pros of targeting PL^{pro}. Signal Transduction and Targeted Therapy 5, 223. https://doi.org/10.1038/s41392-020-00335-z

Meeran, M.F.N., Seenipandi, A., Javed, H., Sharma, C., Hashiesh, H.M., Goyal, S.N., Jha, N.K., Ojha, S., 2021. Can limonene be a possible candidate for evaluation as an agent or adjuvant against infection, immunity, and inflammation in COVID-19? Heliyon 7, e05703. https://doi.org/10.1016/j.heliyon.2020.e05703

Mehrbod, P., Hudy, D., Shyntum, D., Markowski, J., Łos, M.J., Ghavami, S., 2020. Quercetin as a natural therapeutic candidate for

the treatment of influenza virus. Biomolecules 11, 10. https://doi.org/10.3390/biom11010010

Mieres-Castro, D., Ahmar, S., Shabbir, R., Mora-Poblete, F., 2021. Antiviral activities of *Eucalyptus* essential oils: Their effectiveness as therapeutic targets against human viruses. Pharmaceuticals 14, 1210. https://doi.org/10.3390/ph14121210

Minami, A., Kurebayashi, Y., Takahashi, T., Otsubo, T., Ikeda, K., Suzuki, T., 2021. The function of sialidase revealed by sialidase activity imaging probe. International Journal of Molecular Sciences 22, 3187. https://doi.org/10.3390/ijms22063187

Molteni, C.G., Principi, N., Esposito, S., 2014. Reactive oxygen and nitrogen species during viral infections. Free Radical Research 48, 1163–1169. https://doi.org/10.3109/10715762.2014.945443

Montenegro-Landívar, M.F., Tapia-Quirós, P., Vecino, X., Reig, M., Valderrama, C., Granados, M., Cortina, J.L., Saurina, J., 2021. Polyphenols and their potential role to fight viral diseases: An overview. Science of The Total Environment 801, 149719. https://doi.org/10.1016/j.scitotenv.2021.149719

Morimoto, H., Hatanaka, T., Narusaka, M., Narusaka, Y., 2022. Molecular investigation of proanthocyanidin from *Alpinia zerumbet* against the influenza A virus. Fitoterapia 158, 105141. https://doi.org/10.1016/j.fitote.2022.105141

Narayanan, A., Narwal, M., Majowicz, S.A., Varricchio, C., Toner, S.A., Ballatore, C., Brancale, A., Murakami, K.S., Jose, J., 2022. Identification of SARS-CoV-2 inhibitors targeting M^{pro} and PL^{pro} using in-cell-protease assay. Communications Biology 5, 169. https://doi.org/10.1038/s42003-022-03090-9

Nelson, P.P., Papadopoulos, N.G., Skevaki, C., 2022. Respiratory viral pathogens, in: Encyclopedia of Respiratory Medicine. Elsevier, pp. 129–137. https://doi.org/10.1016/B978-0-12-801238-3.11635-6

Oriola, A.O., Oyedeji, A.O., 2022. Essential oils and their compounds as potential anti-influenza agents. Molecules 27, 7797. https://doi.org/10.3390/molecules27227797

Oxford, J.S., Lambkin, R., Gibb, I., Balasingam, S., Chan, C., Catchpole, A., 2005. A throat lozenge containing amyl meta cresol and dichlorobenzyl alcohol has a direct virucidal effect on respiratory syncytial virus, influenza A and SARS-CoV. Antiviral Chemistry and Chemotherapy 16, 129–134. https://doi.org/10.1177/095632020501600205

Özen, T., Kinalioğlu, K., 2008. Determination of antioxidant activity of various extracts of *Parmelia saxatilis*. Biologia (Bratisl) 63, 211–216. https://doi.org/10.2478/s11756-008-0047-6

Pizzino, G., Irrera, N., Cucinotta, M., Pallio, G., Mannino, F., Arcoraci, V., Squadrito, F., Altavilla, D., Bitto, A., 2017. Oxidative stress: harms and benefits for human health. Oxidative Medicine and Cellular Longevity 2017, 1–13. https://doi.org/10.1155/2017/8416763

Rahmani, S., Naraki, K., Roohbakhsh, A., Hayes, A.W., Karimi, G., 2023. The protective effects of rutin on the liver, kidneys, and heart by counteracting organ toxicity caused by synthetic and natural compounds. Food Science and Nutrition 11, 39–56. https://doi.org/10.1002/fsn3.3041

Rajurkar, N., Hande, S., 2011. Estimation of phytochemical content and antioxidant activity of some selected traditional Indian medicinal plants. Journal of Pharmaceutical Sciences 73, 146. https://doi.org/10.4103/0250-474X.91574

Ramulondi, M., de Wet, H., van Vuuren, S., 2019. Toxicology of medicinal plants and combinations used in rural northern KwaZulu-Natal (South Africa) for the treatment of hypertension. Journal of Herbal Medicine 16, 100251. https://doi.org/10.1016/j.hermed.2018.12.001

Rants'o, T.A., Johan van der Westhuizen, C., van Zyl, R.L., 2022a. Optimization of covalent docking for organophosphates interaction with *Anopheles* acetylcholinesterase. Journal of Molecular Graphics and Modelling 110, 108054–108065. https://doi.org/10.1016/j.jmgm.2021.108054

Rants'o, T.A., Koekemoer, L.L., van Zyl, R.L., 2023. *In vitro* and *in silico* analysis of the *Anopheles* anticholinesterase activity of terpenoids. Parasitology International 93, 102713–102726. https://doi.org/10.1016/j.parint.2022.102713

Rants'o, T.A., van Greunen, D.G., van der Westhuizen, C.J., Riley, D.L., Panayides, J.-L., Koekemoer, L.L., van Zyl, R.L., 2022b. The *in silico* and *in vitro* analysis of donepezil derivatives for *Anopheles* acetylcholinesterase inhibition. PLoS One 17, e0277363–e0277375. https://doi.org/10.1371/journal.pone.0277363

Reichling, J., 2022. Antiviral and virucidal properties of essential oils and isolated compounds – A scientific approach. Planta Med 88, 587–603. https://doi.org/10.1055/a-1382-2898

Ribaudo, G., Yun, X., Ongaro, A., Oselladore, E., Ng, J.P.L., Haynes, R.K., Law, B.Y.K., Memo, M., Wong, V.K.W., Coghi, P., Gianoncelli, A., 2023. Combining computational and experimental evidence on the activity of antimalarial drugs on papain-like protease of SARS-CoV-2: A repurposing study. Chemical Biology & Drug Design 101, 809–818. https://doi.org/10.1111/cbdd.14187

Sandner, G., Heckmann, M., Weghuber, J., 2020. Immunomodulatory activities of selected essential oils. Biomolecules 10, 1139. https://doi.org/10.3390/biom10081139

Sang, H., Huang, Y., Tian, Y., Liu, M., Chen, L., Li, L., Liu, S., Yang, J., 2021. Multiple modes of action of myricetin in influenza A virus infection. Phytotherapy Research 35, 2797–2806. https://doi.org/10.1002/ptr.7025

Sanz-Leon, P., Hamilton, L.H.W., Raison, S.J., Pan, A.J.X., Stevenson, N.J., Stuart, R.M., Abeysuriya, R.G., Kerr, C.C., Lambert, S.B., Roberts, J.A., 2022. Modelling herd immunity requirements in Queensland: Impact of vaccination effectiveness, hesitancy and variants of SARS-CoV-2. Philosophical Transactions of the Royal Society A: Mathematical, Physical and Engineering Sciences 380, 20210311. https://doi.org/10.1098/rsta.2021.0311

Schallreuter, K.U., Salem, M.A.E.L., Gibbons, N.C.J., Maitland, D.J., Marsch, E., Elwary, S.M.A., Healey, A.R., 2012. Blunted epidermal L-tryptophan metabolism in vitiligo affects immune response and ROS scavenging by Fenton chemistry, part 2: epidermal H_2O_2/$ONOO^-$ mediated stress in vitiligo hampers indoleamine 2,3-dioxygenase and aryl hydrocarbon receptor-mediated immune response signaling. The FASEB Journal 26, 2471–2485. https://doi.org/10.1096/fj.11-201897

Sebaugh, J.L., 2011. Guidelines for accurate EC50/IC50 estimation. Pharm Stat 10, 128–134. https://doi.org/10.1002/pst.426

Setzer, W., 2016. Essential oils as complementary and alternative medicines for the treatment of influenza. American Journal of Essential Oils and Natural Products 4, 16–22.

Shao, J., Yin, Z., Wang, Y., Yang, Y., Tang, Q., Zhang, M., Jiao, J., Liu, C., Yang, M., Zhen, L., Hassouna, A., White, W.L., Lu, J., 2020. Effects of different doses of *Eucalyptus* oil from *Eucalyptus globulus* Labill on respiratory tract immunity and immune function in healthy rats. Frontiers in Pharmacology 11, 1287. https://doi.org/10.3389/fphar.2020.01287

Shoker, R.M.H., Al-Shammery, W.H., Al-Aidy, S.R., 2023. A review article: Free radical and replacement synthetic antioxidant by natural antioxidant. Journal for Research in Applied Sciences and Biotechnology 2, 206–211. https://doi.org/10.55544/jrasb.2.2.29

Suriyatem, R., Auras, R., Intipunya, P., Rachtanapun, P., 2017. Predictive mathematical modeling for EC50 calculation of antioxidant activity and antibacterial ability of Thai bee products. Journal of Applied Pharmaceutical Science 7, 122-133. https://doi.org/10.7324/JAPS.2017.70917

Tambe, V., Bhambar, R., 2014. Estimation of total phenol, tannin, alkaloid and flavonoid in *Hibiscus Tiliaceus* Linn. wood extracts. Journal of Pharmacognosy and Phytochem 2, 2321–6182.

Ti, H., 2021. Phytochemical profiles and their anti-inflammatory responses against influenza from traditional Chinese medicine or herbs. Mini-Reviews in Medicinal Chemistry 20, 2153–2164. https://doi.org/10.2174/1389557520666200807134921

Touazi, A.A., Boussaadia, A., Didaoui, S., Nasrallah, N., Chelghoum, F., Benziane, M., 2024. Measurement and modeling of excess molar volume and excess enthalpy of n-tridecane or n-tetradecane with decalin by application of PFP theory . Journal of Solution Chemistry 53, 1246–1268. https://doi.org/10.1007/s10953-024-01374-8

Tsamo, D.L.F., Tamokou, J.-D.-D., Kengne, I.C., Ngnokam, C.D.J., Djamalladine, M.D., Voutquenne-Nazabadioko, L., Ngnokam, D., 2021. Antimicrobial and antioxidant secondary metabolites from *Trifolium baccarinii* Chiov. (Fabaceae) and their mechanisms of antibacterial action. Biomed Research International 2021, 1–15. https://doi.org/10.1155/2021/3099428

Tuffery, P., Derreumaux, P., 2012. Flexibility and binding affinity in protein–ligand, protein–protein and multi-component protein interactions: limitations of current computational approaches. Journal of The Royal Society Interface 9, 20–33.

Tyagi, A.K., Malik, A., 2011. Antimicrobial potential and chemical composition of *Eucalyptus globulus* oil in liquid and vapour phase against food spoilage microorganisms. Food Chemistry 126, 228–235. https://doi.org/10.1016/j.foodchem.2010.11.002

Vambe, M., Aremu, A.O., Chukwujekwu, J.C., Finnie, J.F., Van Staden, J., 2018. Antibacterial screening, synergy studies and phenolic content of seven South African medicinal plants against drug-sensitive and resistant microbial strains. South African Journal of Botany 114, 250–259. https://doi.org/10.1016/j.sajb.2017.11.011

van der Westhuizen, C.J., Stander, A., Riley, D.L., Panayides, J.-L., 2022. Discovery of novel acetylcholinesterase inhibitors by virtual screening, *in vitro* Screening, and molecular dynamics simulations. Journal of Chemical Information and Modelling 62, 1550–1572. https://doi.org/10.1021/acs.jcim.1c01443

Venugopal, P.P., Chakraborty, D., 2022. Molecular mechanism of inhibition of COVID-19 main protease by β-adrenoceptor agonists and adenosine deaminase inhibitors using *in silico* methods. Journal of Biomolecular Structure and Dynamics 40, 5112–5127. https://doi.org/10.1080/07391102.2020.1868337

Wallace, L.E., de Vries, E., van Kuppeveld, F.J.M., de Haan, C.A.M., 2023. Neuraminidase-dependent entry of influenza A virus is determined by hemagglutinin receptor-binding specificity. Journal of Virology 97, e0060223. https://doi.org/10.1128/jvi.00602-23

Weston, S., Frieman, M.B., 2018. Respiratory viruses, in: Reference Module in Biomedical Sciences. Elsevier. https://doi.org/10.1016/B978-0-12-801238-3.66161-5

Wu, J., 2020. Tackle the free radicals damage in COVID-19. Nitric Oxide 102, 39–41. https://doi.org/10.1016/j.niox.2020.06.002

Wu, Q., Wang, W., Dai, X., Wang, Z., Shen, Z., Ying, H., Yu, C., 2012. Chemical compositions and anti-influenza activities of essential oils from *Mosla dianthera*. Journal of Ethnopharmacology 139, 668–671. https://doi.org/10.1016/j.jep.2011.11.056

Wu, W., Li, R., Li, X., He, J., Jiang, S., Liu, S., Yang, J., 2015. Quercetin as an antiviral agent inhibits influenza A virus (IAV) entry. Viruses 8, 6. https://doi.org/10.3390/v8010006

Yan, A., Li, W., Zhao, X., Cao, R., Li, H., Chen, L., Li, X., 2024. Noncovalent SARS-CoV-2 main protease inhibitors: A virtual screening and molecular dynamic simulation study. Results in Chemistry 7, 1–10. https://doi.org/10.1016/j.rechem.2024.101428